






Title	Uncoordinated centrosome cycle underlies the instability of non-diploid somatic cells in mammals
Author(s)	Yaguchi, Kan, Yamamoto, Takahiro, Matsui, Ryo, Takeda, Yuki, Shibamura, Aki, Tsuko, Kaninura, Eiko, Oda, Toshiaki, Uehara, Ryota
Citation	Journal of cell biology 217(7):2463-2483 <a href="https://doi.org/10.1083/jcb.201701151">https://doi.org/10.1083/jcb.201701151</a>
Issue Date	2018-07
Doc URL	<a href="http://hdl.handle.net/2115/71788">http://hdl.handle.net/2115/71788</a>
Rights	Uehara, Ryota et al. 2018. Originally published in JOURNAL OF CELL BIOLOGY. doi:10.1083/jcb.201701151
Rights URL	<a href="https://creativecommons.org/licenses/by/nc-sa/4.0/">https://creativecommons.org/licenses/by/nc-sa/4.0/</a>
Type	article
File Information	2463.full.pdf



[Instructions for use](#)

ARTICLE

# Uncoordinated centrosome cycle underlies the instability of non-diploid somatic cells in mammals

Kan Yaguchi<sup>1</sup>, Takahiro Yamamoto<sup>1\*</sup>, Ryo Matsui<sup>1\*</sup>, Yuki Tsukada<sup>2</sup> , Atsuko Shibamura<sup>3</sup>, Keiko Kamimura<sup>1</sup>, Toshiaki Koda<sup>1,4</sup> , and Ryota Uehara<sup>1,3,4</sup> 

**In animals, somatic cells are usually diploid and are unstable when haploid for unknown reasons. In this study, by comparing isogenic human cell lines with different ploidies, we found frequent centrosome loss specifically in the haploid state, which profoundly contributed to haploid instability through subsequent mitotic defects. We also found that the efficiency of centriole licensing and duplication changes proportionally to ploidy level, whereas that of DNA replication stays constant. This caused gradual loss or frequent overduplication of centrioles in haploid and tetraploid cells, respectively. Centriole licensing efficiency seemed to be modulated by astral microtubules, whose development scaled with ploidy level, and artificial enhancement of aster formation in haploid cells restored centriole licensing efficiency to diploid levels. The ploidy-centrosome link was observed in different mammalian cell types. We propose that incompatibility between the centrosome duplication and DNA replication cycles arising from different scaling properties of these bioprocesses upon ploidy changes underlies the instability of non-diploid somatic cells in mammals.**

## Introduction

Animal species generally have diplontic life cycles, where somatic cell division occurs only during the diploid phase. Exceptionally, haploid or near-haploid animal somatic cells arise through activation of oocytes without fertilization or because of aberrant chromosome loss during tumorigenesis (Wutz, 2014). However, haploidy in animal somatic cells is generally unstable, and haploid cells in a wide variety of species, including insects, amphibians, and mammals, convert to diploid through doubling of the whole genome during successive culture for several weeks both in vitro and in vivo (Freed, 1962; Kaufman, 1978; Debec, 1984; Kotecki et al., 1999; Elling et al., 2011; Leeb and Wutz, 2011; Yang et al., 2013; Essletzbichler et al., 2014; Li et al., 2014; Sagi et al., 2016). This is in sharp contrast to plants and lower eukaryotic organisms, in which haploid somatic cells can proliferate stably (Mable and Otto, 1998; Forster et al., 2007). This raises the possibility that, specifically in animals, the cell replication mechanism is stringently adapted to the diploid state and becomes compromised in haploid cells; however, the physiological impacts of ploidy differences on animal cell replication processes remain largely unknown.

In animal cells, control of centrosome number is essential for precise cell replication. During mitosis, pairs of centrosomes serve as major microtubule (MT) organizing centers for bipolar

spindle formation, and irregular numbers of centrosomes form spindles with abnormal polarities, endangering proper chromosome segregation (Gönczy, 2015). Centrosome number control is achieved through elaborate regulation of the centrosome duplication cycle (Loncarek and Bettencourt-Dias, 2018). Upon exit from mitosis, an engaged pair of centrioles comprising a centrosome separate from one another, producing two centrosomes (Kuriyama and Borisy, 1981). This centriole disengagement process is a prerequisite for “licensing” each preexisting centriole to serve as a template for the formation of a daughter centriole in the subsequent cell cycle (Tsou and Stearns, 2006; Tsou et al., 2009). A scaffold protein, Cep152, accumulates on the licensed preexisting centrioles, subsequently recruiting a key centriole duplication regulator, Polo-like kinase 4 (Plk4; Cizmecioglu et al., 2010; Dzhindzhev et al., 2010; Hatch et al., 2010; Kim et al., 2013; Sonnen et al., 2013; Fu et al., 2016). Plk4, in turn, mediates the recruitment of SAS-6 on the outside wall of the preexisting centrioles to form the procentriolar cartwheel, which founds the basis for the subsequent elongation of daughter centrioles (Bettencourt-Dias et al., 2005; Habedanck et al., 2005; Leidel et al., 2005; Kleylein-Sohn et al., 2007; Nakazawa et al., 2007; Dzhindzhev et al., 2014; Fong et al., 2014; Ohta et al., 2014; Moyer et al., 2015). Importantly, there are striking similarities between

<sup>1</sup>Graduate School of Life Science, Hokkaido University, Sapporo, Japan; <sup>2</sup>Division of Biological Science, Graduate School of Science, Nagoya University, Nagoya, Japan; <sup>3</sup>Creative Research Institution, Hokkaido University, Sapporo, Japan; <sup>4</sup>Faculty of Advanced Life Science, Hokkaido University, Sapporo, Japan.

\*T. Yamamoto and R. Matsui contributed equally to this paper; Correspondence to Ryota Uehara: [ruehara@sci.hokudai.ac.jp](mailto:ruehara@sci.hokudai.ac.jp).

© 2018 Yaguchi et al. This article is distributed under the terms of an Attribution–Noncommercial–Share Alike–No Mirror Sites license for the first six months after the publication date (see <http://www.rupress.org/terms/>). After six months it is available under a Creative Commons License (Attribution–Noncommercial–Share Alike 4.0 International license, as described at <https://creativecommons.org/licenses/by-nc-sa/4.0/>).

the molecular mechanisms governing temporal regulation of the centriole duplication cycle and DNA replication cycle. A mitotic kinase, Plk1, and a cysteine endoprotease, separase, cooperatively regulate resolution of the connections of the engaged centrioles or paired sister chromatids during or at the end of mitosis, and cyclin E-cdk2 controls the initiation of both centriole duplication and DNA replication during G1/S phase (Matsumoto et al., 1999; Meraldi et al., 1999; Coverley et al., 2002; Nasmyth, 2002; Sumara et al., 2002; Tsou and Stearns, 2006; Tsou et al., 2009). These regulatory mechanisms ensure precise temporal coordination between these two cellular processes, allowing cells to possess a constant number of centrosomes throughout numerous rounds of cell cycles during proliferation.

To determine the cellular processes affected by ploidy difference and understand the origin of intolerance of somatic haploidy in animal cells, we performed side-by-side comparisons of cell replication in isogenic mammalian somatic cells with different ploidy levels. We found that the efficiency of centrosome cycle progression scales proportionally with ploidy level, which uncouples the progression of the centrosome cycle from that of the DNA cycle and compromises centrosome number control in non-diploid states.

## Results

### Haploidy-specific mitotic defects in human somatic cells

To investigate the effect of ploidy differences on the cell replication process, we used the near-haploid human cell line, HAP1 (Carette et al., 2011). As previously reported, the haploid state of this cell line was unstable, and almost all cells in haploid-enriched culture diploidized over several weeks of passage (Fig. 1A; Essletzichler et al., 2014). Diploidized cells were significantly larger than haploid cells (Fig. 1B and Fig. S1, A–C); therefore, we could purify the isogenic haploid and diploid cell populations separately for side-by-side comparisons using size-based sorting.

We first compared the progression of the cell cycle and cell division in haploid and diploid cells using live imaging (Fig. 1, C–F; and Videos 1, 2, and 3). Mean cell cycle length was significantly greater in haploid than in diploid cells ( $806 \pm 212$  and  $714 \pm 186$  min, respectively;  $n > 282$ ;  $P < 10^{-8}$ ,  $t$  test; Fig. 1D). We also found that 72 of 1,181 haploid cells (6.0%) showed a severe mitotic delay, spending  $>50$  min in the mitotic phase (Fig. 1, C, E, and F). Of the mitotically arrested haploid cells, 36 entered anaphase and completed cytokinesis, whereas 20 died during mitosis, and the remaining 7 exited the mitotic phase without chromosome segregation (mitotic slippage; Fig. 1, C and F; and Video 2). Importantly, these defects were scarcely observed in diploid cells (Fig. 1F and Video 3).

Because mitotic slippage doubles DNA content, it can affect haploid stability, even when it occurs at low frequency. We therefore estimated the potential contribution of haploid-specific mitotic defects to haploid instability using a mathematical cell population transition model (described in Materials and methods; source code files are provided in the online supplemental material). In this model, haploid or diploid cells proliferate exponentially, with respective doubling times corresponding to measured cell cycle lengths. Haploid cells die or diploidize through mitotic

death or mitotic slippage, respectively, with empirically observed frequencies (Fig. 1F). A simulated time course of a haploid population using the model was essentially consistent with the experimentally observed diploidization profiles (Fig. 1G). In the simulation, mitotic slippage at the observed order of frequency could account solely for  $\sim 40\%$  of haploid population loss during 60 d of culture, and haploid stability was sensitive to small changes in the frequency of mitotic slippage (Figs. 1G and S1D). Based on the above experimental and theoretical analyses, we propose the following mechanism for haploid instability: haploid-specific cell division failure drives chronic conversion of haploid cells into diploid, which is accompanied by preferential expansion of the diploid population because of its cell-autonomous growth advantage over haploid cells. Because haploid-specific mitotic defects are likely to contribute profoundly to haploid instability, we decided to investigate the cellular mechanisms underlying them.

### Frequent centrosome loss and monopolar spindle formation in haploid human somatic cells

To determine the cause of haploid-specific mitotic defects, we investigated the organization of the mitotic spindle in haploid and diploid cells by  $\alpha$ -tubulin immunostaining. Whereas the majority of diploid cells possessed bipolar spindles,  $\sim 25\%$  ( $n = 3$ ) of haploid cells had monopolar spindles (Fig. 2, A and B). Consistently, whereas the majority of diploid mitotic cells had a pair of centrosomes, each of which consisted of two centrioles, we observed loss of centrosomes and centrioles in  $>20\%$  of haploid mitotic cells (visualized by  $\gamma$ -tubulin and centrin immunostaining, respectively; Fig. 2, C and D; and Fig. S1E). Even when 10 individual clonal subpopulations were isolated from haploid cell culture by single-cell sorting, the frequent spindle monopolarization and centrosome loss were observed in all these haploid clones (Fig. S1F). This suggests that the entire population of haploid cells potentially lose their centrosomes over time. Because these haploid and diploid cells were isogenic, the frequent centrosome loss in haploid cells must be a consequence of haploidy rather than genetic background.

To examine the relationship between spindle disorganization and mitotic defects in haploid cells, we performed live imaging using haploid HAP1 cells stably expressing EGFP- $\alpha$ -tubulin (Fig. 2, E and F; Fig. S1G; and Videos 4, 5, and 6). Of 1,264 cells that entered mitosis, 118 (9.3%) formed monopolar spindles, and of these monopolar cells, 19 later bipolarized and completed mitosis (Fig. 2E, arrowhead; and Video 5), 48 died in mitosis, and 9 underwent mitotic slippage (Fig. 2, E and F; and Video 6). Importantly, all mitotic slippage events and the majority of mitotic deaths accompanied spindle monopolarization. These results suggest that spindle disorganization caused by haploid-specific centrosome loss makes a major contribution to the mitotic defects in haploid cells.

### Cells are more susceptible to centrosome loss in the haploid state than in the diploid state

In general, animal somatic cells without centrosomes can still form bipolar spindles and complete mitosis, albeit with reduced fidelity (Khodjakov et al., 2000; Khodjakov and Rieder, 2001; Sir et al., 2013). The fact that haploid cells suffer from frequent

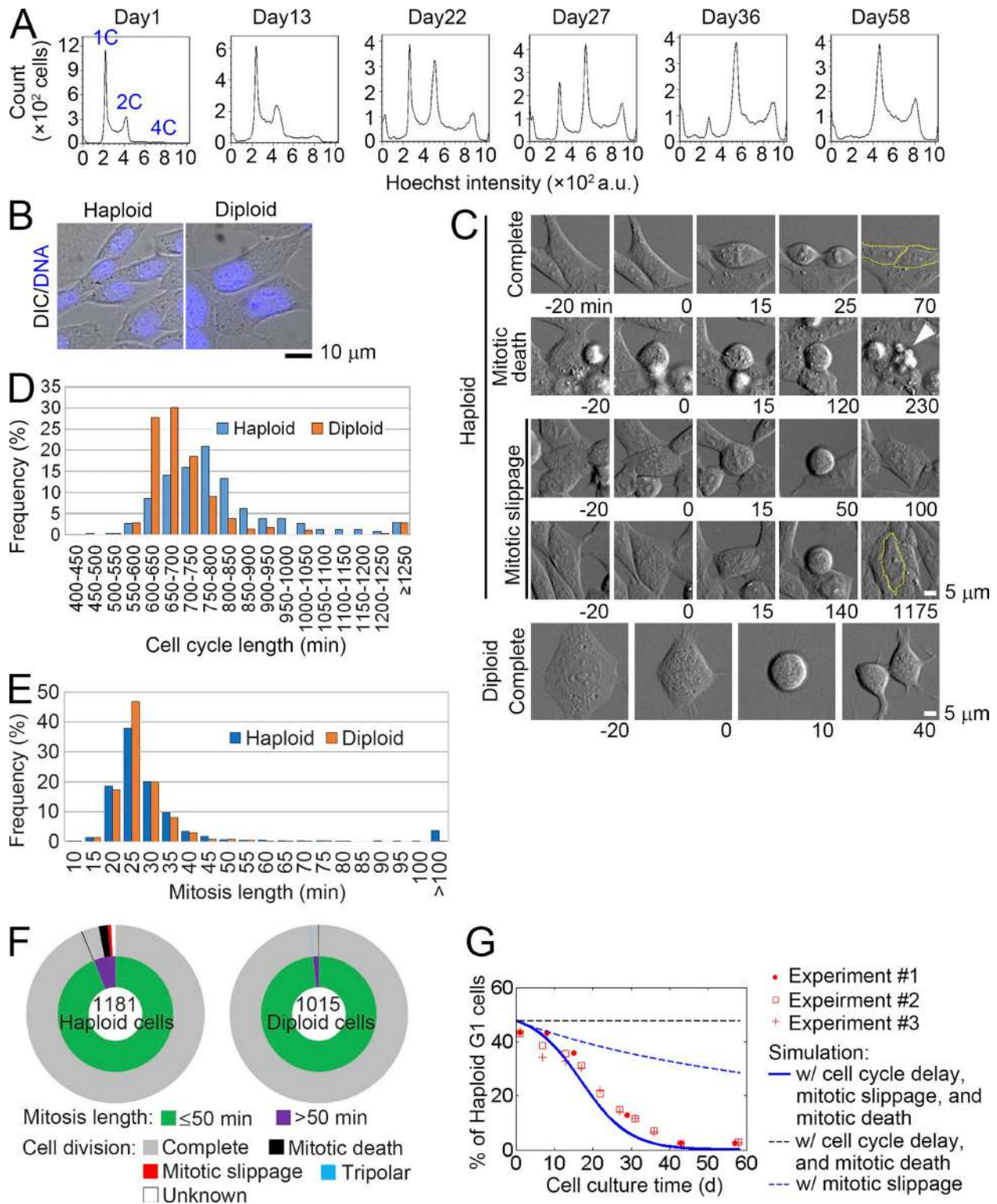


**Figure 1. Haploid-specific mitotic defects and subsequent diploidization in HAP1 cells.** (A) Flow cytometric analysis of DNA content in Hoechst-stained cells during long-term culture. Representative data from three independent experiments are shown. (B) Hoechst-stained haploid and diploid cells. (C) Live images of haploid and diploid cells taken at 5-min intervals. Nuclear envelope breakdown (NEBD) was set as 0 min. Arrowhead indicates mitotic death. Broken lines mark cell boundaries. (D and E) Distribution of cell cycle length (from one NEBD to the next NEBD) or mitotic duration (from NEBD to anaphase onset) quantified from 339 haploid and 285 diploid (D) and 1,180 haploid and 1,015 diploid cells (E), respectively. Data are from at least two independent experiments. (F) Classification of mitotic defects (outer circle) sorted by mitotic duration (inner circle) determined based on analysis of 1,181 haploid and 1,015 diploid cells in at least two independent experiments. (G) Time course of the haploid G1 fraction during long-term culture of haploid-enriched cells in A. Data from three independent experiments are compared with theoretical model simulations.

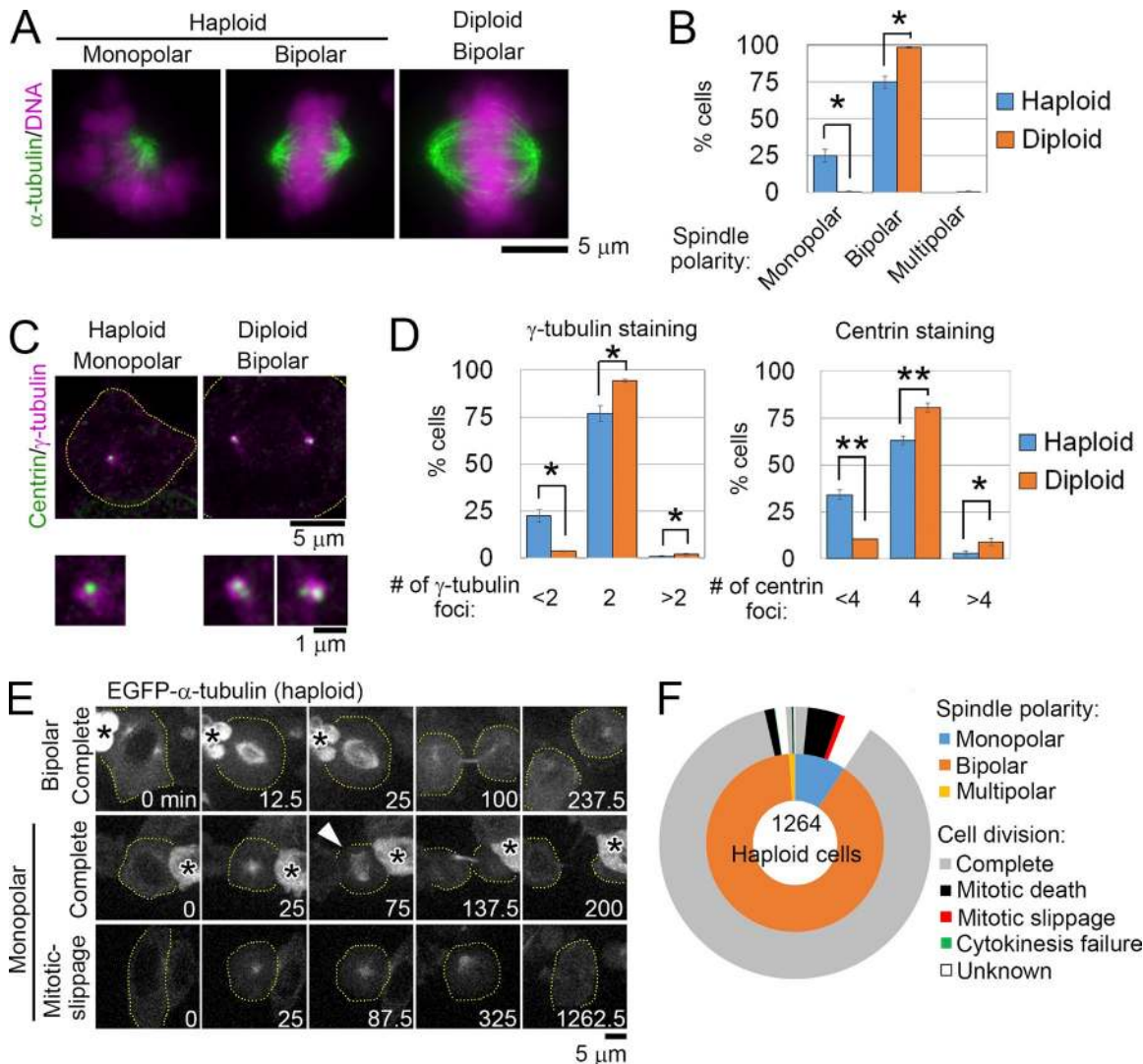


**Figure 2. Centrosome loss and monopolar spindle formation in haploid HAP1 cells.** (A and C) Immunostaining of  $\alpha$ -tubulin and chromosomes (stained using DAPI; A), or  $\gamma$ -tubulin and centrin (C) in haploid and diploid mitotic cells. Enlarged images (3 $\times$ ) of centrosomes are shown at bottom in C. (B and D) Frequency of spindle polarities (B) and centrosome or centriole numbers (D) in A and C, respectively. Values represent means  $\pm$  standard error (SE) of three independent experiments (\*,  $P < 0.05$ ; \*\*,  $P < 0.01$ ,  $t$  test). At least 159 (B) or 302 cells (D) were analyzed per condition. (E) Live images of haploid EGFP- $\alpha$ -tubulin cells taken at 12.5-min intervals. NEBD was set as 0 min. Arrowhead indicates an acentrosomal pole newly formed from a monopolar spindle. Broken lines show cell boundaries. Asterisks mark neighboring cells. (F) Classification of mitotic defects (outer circle) sorted by spindle polarities (inner circle) determined by analysis of 1,264 haploid EGFP- $\alpha$ -tubulin cells from five independent experiments. Cells that moved out of the field of view during the mitotic phase were categorized as unknown.

monopolar spindle formation and mitotic failure upon centrosome loss raises the possibility that cells are particularly susceptible to centrosome loss in the haploid state. To test this possibility, we performed live imaging of haploid and diploid HAP1 cells stably expressing GFP-centrin that were pretreated with a Plk4 inhibitor (centrinone B) for 1 d (Fig. 3, A and B; and Fig. S1 H; Wong et al., 2015). Pretreatment reduced the number of GFP-centrin foci to the same extent (to less than 3) in haploid and diploid cells. Approximately 35% or 11% of centrinone B-treated haploid cells (38 or 12 out of 105 mitotic cells, respectively) showed mitotic death or slippage, respectively. On the contrary, the effect of centrosome loss on mitotic progression was milder in diploid than in haploid cells; ~18% of the centrinone B-treated diploid cells (20 out of 113 cells) showed mitotic death, which was similar to those

reported in other cell lines (Wong et al., 2015), and only 2.6% of these cells (3 out of 113 cells) showed mitotic slippage. We also investigated the impact of the centrinone B-induced centrosome loss on the stability of the haploid or diploid state in HAP1 cells (Fig. 3 C). Interestingly, although DNA content remained almost unchanged after 4 d centrinone B treatment in diploid cells, large populations of haploid cells were converted to the diploid state under the same experimental condition. These results suggest that the haploid state is particularly susceptible to centrosome loss, which, in combination with the haploidy-linked centrosome loss, causes frequent mitotic failure and haploid instability. We observed that diploid HAP1 cells, similar to other cell lines such as HeLa or DLD-1 cells, continued to grow upon chronic centrosome loss after prolonged (>14 d) centrinone B treatment, eliminating

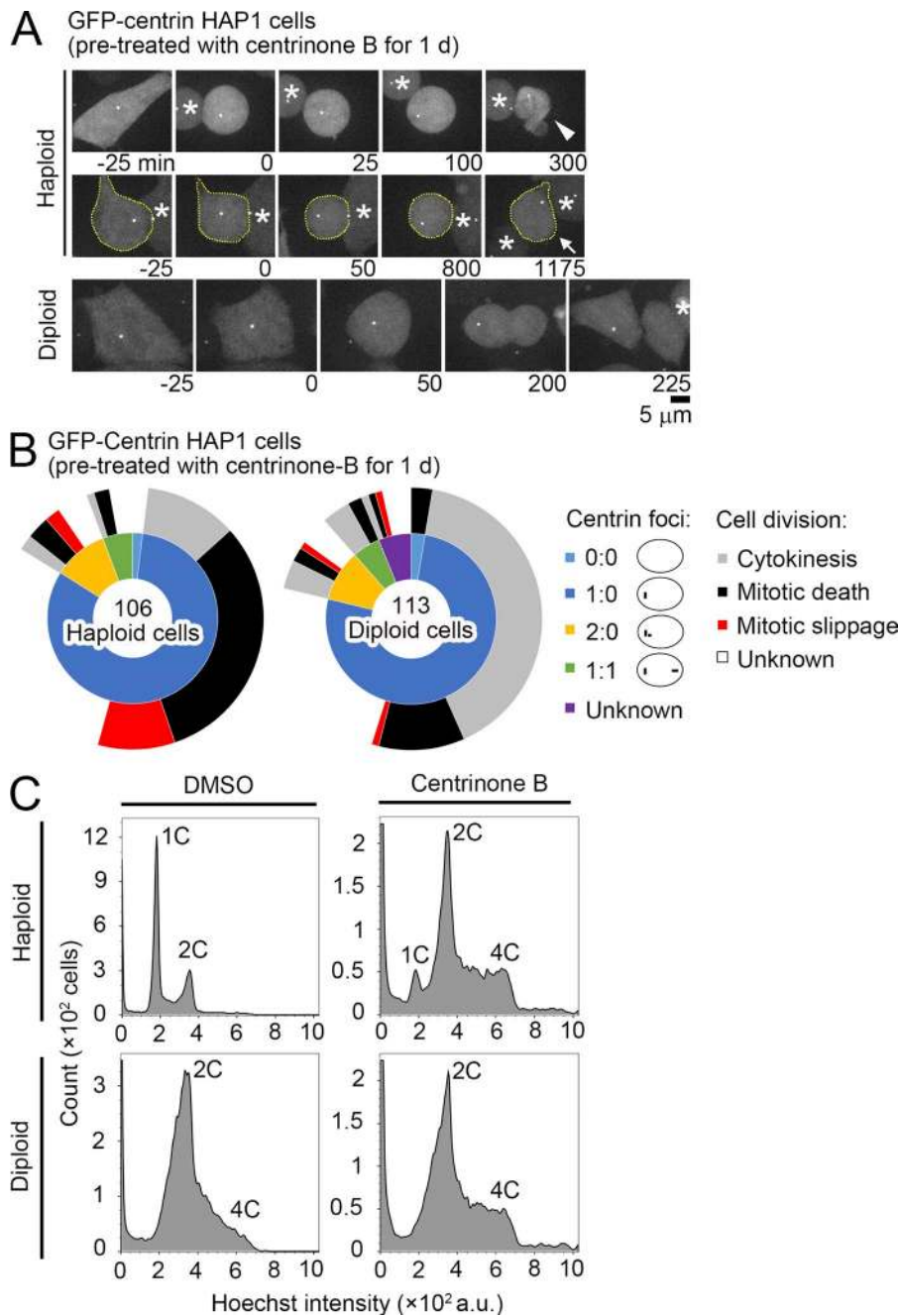


**Figure 3. Haploid cells are more susceptible to centrosome loss than diploid cells.** (A) Live images of haploid or diploid GFP-centrin cells pre-treated with 500 nM centrinone B for 1 d. Images were taken at 25-min intervals. Mitotic entry was set as 0 min. Arrowhead or arrow indicates mitotic death or mitotic slippage, respectively. Broken lines show cell boundaries. Asterisks mark neighboring cells. (B) Classification of mitotic defects (outer circle) sorted by centriole content (inner circle) determined by live imaging of GFP-centrin cells in A. Data are from two independent experiments. Mitotic cells that moved out of the field of view or did not exit mitosis by the end of imaging were categorized as unknown. (C) Flow cytometric analysis of DNA content in Hoechst-stained cells pretreated with or without 500 nM centrinone B for 4 d. Representative data from two independent experiments are shown.

the possibility that the cell-type-specific background of HAP1 cells renders them particularly vulnerable to centrosome loss (Fig. S1, I and J).

**Centriole duplication efficiency scales proportionally with ploidy level**

To understand how haploid cells lose their centrosomes, we next tested the progression of centriole duplication in haploid and diploid cells. Cells were synchronized by mitotic shake-off after release from nocodazole arrest, and DNA replication and centriole duplication in the subsequent cell cycle was monitored by BrdU incorporation and counting of immunostained centrin-positive foci, respectively (Fig. 4, A-C; and Fig. S2 A). BrdU incorporation in haploid cells was slightly slower than that in

diploids; however, it reached the same maximum level within 8 h of nocodazole release (Fig. 4 A). In contrast, the progression of centriole duplication was drastically delayed in haploid cells relative to that in diploids. Centriole duplication started ~5 h after nocodazole release, and cells with four centrosomes predominated at 8 h after nocodazole release in diploid cells, whereas ~65% ( $n = 3$ ) of haploid cells had unduplicated centrosomes at that time (Fig. 4, B and C). When the duration of the S phase was extended by thymidine treatment after nocodazole release, the percentage of duplicated pairs of centrosomes in haploid cells increased monotonically, reaching a maximum level equivalent to that in diploids within 16 h after the addition of thymidine (Fig. S2 B). Hence, centriole duplication was not completely compromised in haploid cells; rather, it became too inefficient to keep pace with

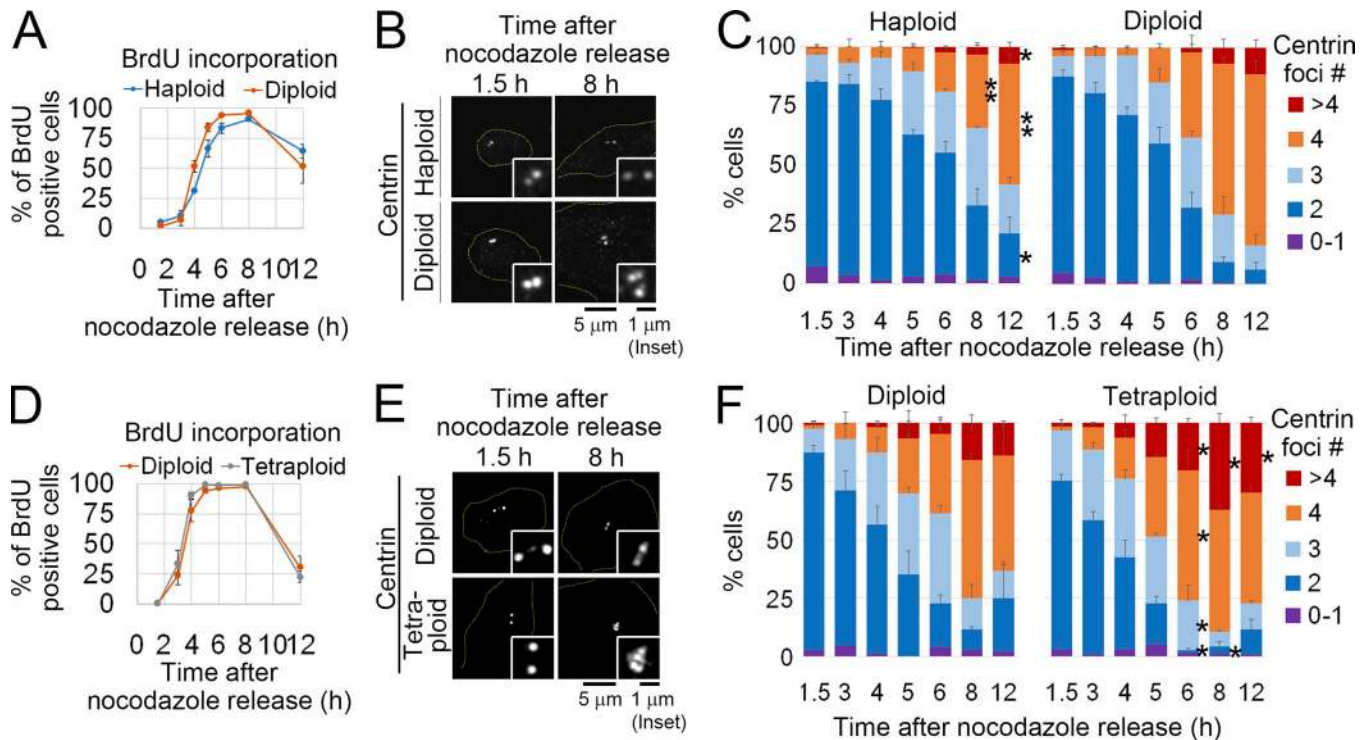


**Figure 4. Centriole duplication efficiency scales to ploidy level in HAP1 cells.** (A and D) BrdU incorporation after nocodazole release in cells with different ploidy levels. Mean  $\pm$  SE of three independent experiments. At least 1,258 (A) or 818 cells (D) were analyzed for each data point. (B and E) Immunostaining of centrioles in synchronized cells with different ploidy levels. Insets show 3 $\times$  enlarged images of centrioles. Broken lines show cell boundaries. (C and F) Percentages of cells with indicated numbers of centriole foci at each time point after nocodazole release. Values represent means  $\pm$  SE of three independent experiments (asterisks indicate significant differences from diploid cells; \*,  $P < 0.05$ ; \*\*,  $P < 0.01$ ,  $t$  test). At least 170 (C) or 87 cells (F) were analyzed for each data point. Note that centriole foci number decreased from 8 h to 12 h after nocodazole release in some cases, because some population of cells divided during that time.

the DNA replication cycle, resulting in gradual loss of centrioles in successive cell cycles. The delay in centriole duplication in haploid cells was also observed in the asynchronous condition using correlative live- and fixed-cell imaging (Fig. 8; Materials and methods), thereby eliminating the possibility of side effects of cell synchronization.

Next, we determined whether an increase in ploidy from diploid could also affect centriole duplication efficiency. We established stable tetraploid HAP1 cell lines by doubling the whole genomes of diploid cells (Fig. S2 C; Materials and methods). The majority (~72%,  $n = 3$ ) of tetraploid cells had two mother centrioles when synchronized in the G1 phase, suggesting that excess centrosomes obtained upon tetraploidization were lost during subsequent cloning, as reported for other cell lines (Fig. 4, D-F; Ganem et al., 2009; Potapova et al., 2016). The progression of BrdU incorporation after nocodazole release was similar between diploid and tetraploid cells (Figs. 4 D and S2 D); however, centriole duplication progressed significantly faster in tetraploid cells than that in diploid cells (Fig. 4, E and F). We observed centriole overduplication significantly more often in tetraploid cells than in diploid cells (Fig. 4 F). Up-regulation of centriole duplication and formation of the supernumerary centrioles in tetraploid cells were also observed in the asynchronous cell culture condition in correlative live- and fixed-cell imaging (see Fig. 8). Long-term live imaging using GFP-centrin HAP1 cells demonstrated that a substantial population of tetraploid cells that possessed supernumerary centrioles at mitotic entry completed cell division,

resulting in ~8% tetraploid daughter cells entering the next cell cycle with excess numbers of centrioles (Fig. S2, E-G). Consistent with this, the mean centriole number in an asynchronous culture of tetraploid HAP1 cells was significantly higher than that in diploid cells ( $3.2 \pm 0.9$  and  $2.8 \pm 0.9$  centrioles per cell, respectively;  $n > 87$ ;  $P < 0.01$ ,  $t$  test; Fig. S2 H).

These results above indicate that the efficiency of centriole duplication scaled proportionally with ploidy level, whereas that of DNA replication was relatively insensitive to ploidy. This difference in ploidy dependency potentially threatens centrosome homeostasis upon ploidy conversion (either decreasing or increasing) from diploidy, owing to lack of coordination of these biological processes. To gain insight into the ploidy-dependent up-regulation of centriole duplication among other cell types, we established tetraploid lines from two different nearly diploid human cells, DLD-1 and hTERT RPE-1 (Fig. S3 A). The tetraploidy-linked acceleration of centriole duplication was also observed in DLD-1 cells, but not in RPE-1 cells (Fig. S3, B and C). Consistent with this, mean centriole number was significantly increased in tetraploid DLD-1 cells compared with their diploid counterparts ( $3.5 \pm 1.5$  and  $2.9 \pm 1.1$  centrioles per cell, respectively;  $n > 86$ ;  $P < 0.01$ ,  $t$  test), whereas it was similar between diploid and tetraploid RPE-1 cells ( $2.6 \pm 0.9$  and  $2.8 \pm 0.9$  centrioles per cell, respectively;  $n > 93$ ;  $P = 0.17$ ,  $t$  test; Fig. S3 D). Therefore, the link between centriole duplication and ploidy level is present in cell lines with different tissue origins, although a cell-type-specific difference in its conspicuity might also exist.

### The efficiency of the recruitment of centriole duplication factors changes according to ploidies

Next, we addressed the molecular mechanism by which ploidy difference affects centriole duplication efficiency. For this, we analyzed recruitment of the key duplication factors Cep152, Plk4, and SAS-6 on the preexisting centrioles in haploid, diploid, or tetraploid HAP1 cells synchronized at G1/S phase by nocodazole shake-off (Fig. 5). At early G1 phase (2 h after nocodazole release), Cep152 had already accumulated to more than 50% ( $n = 3$ ) of preexisting centrioles in all ploidies, which is consistent with previous studies reporting that mother centrioles recruit Cep152 from the previous cell cycle (Fig. 5, A and B; Sonnen et al., 2013; Park et al., 2014; Fu et al., 2016). In diploid cells, the majority of preexisting centrioles recruited Cep152 before entry into S phase, but Cep152 recruitment was drastically delayed in haploid cells, and ~35% ( $n = 3$ ) centrioles remained devoid of Cep152 signal, even in early S phase (4 h after nocodazole release; Fig. 5 B). In contrast, Cep152 recruitment was accelerated in tetraploid cells compared with that in diploid cells, with a significant increase in the frequency of Cep152-positive centrioles in early S phase. Because Cep152 is required for the hierarchical recruitment of centriole duplication factors (Kim et al., 2013; Sonnen et al., 2013), the ploidy-dependent changes in its recruitment potentially affect the subsequent processes of centriole biogenesis. Indeed, in haploid or tetraploid cells, recruitment of Plk4 and SAS-6 was delayed or hastened, respectively, compared with those in diploid cells (Fig. 5, C–F). The time gaps in the recruitment of these proteins among different ploidies roughly corresponded with those of daughter centriole formation (Fig. 4, C and F), suggesting that the ploidy-linked shifts in the timing of the sequential recruitment of these key duplication factors during G1 and early S phase change the progression of the entire centriole duplication process among different ploidies. Besides the changes in the timing of their recruitment, we also found that amounts of Cep152 and Plk4 at the centrioles during the S phase (6 h after nocodazole release) changed proportionally with ploidy levels (Fig. S2, I and J).

Previous studies have reported that overexpression of Plk4 overrides the regulatory mechanism that limits daughter centriole number, leading to the formation of excess procentrioles (Bettencourt-Dias et al., 2005; Habedanck et al., 2005; Kleylein-Sohn et al., 2007; Peel et al., 2007). We next determined whether ploidy difference also affects the efficiency of the Plk4-dependent centriole overduplication by transiently expressing GFP-tagged Plk4 in HAP1 cells with different ploidies that were arrested at S phase (Fig. 5, G and H; Materials and methods). Interestingly, the number of daughter centrioles induced by Plk4 overexpression increased with ploidy, with drastic suppression of extra centriole formation in the haploid state. Therefore, the ploidy dependency of the centriole duplication mechanism persisted even in the presence of excess Plk4, suggesting that rate-limiting processes other than Plk4 recruitment may determine the efficiency of the centriole duplication cycle in different ploidy states.

### Centriole licensing is rate limiting for the centriole duplication process in different ploidies

During mitotic exit, the tightly connected mother and daughter centrioles are disengaged, which “licenses” these centrioles to

recruit centriole duplication factors and serve as templates for centriole biogenesis (Tsou and Stearns, 2006; Tsou et al., 2009). Because the centriole licensing through disengagement may potentially be rate limiting for the entire centriole duplication process, we next investigated the effect of ploidy difference on the status of centriole engagement at mitotic exit. For that purpose, a centriole-linking protein, C-Nap1, and centrin were immunostained in asynchronous haploid, diploid, and tetraploid cells (Fig. 6, A and B). Using these markers, engaged centriole pairs are visualized as two adjacent centrin dots flanking a C-Nap1 dot, whereas disengaged pairs are visualized as two centrin dots with two discrete C-Nap1 dots (Tsou and Stearns, 2006). At mitotic exit, during which time two daughter cells were connected by an intercellular bridge after the constriction of the contractile ring, ~25% ( $n = 3$ ) of diploid cells possessed a disengaged centriole pair (Fig. 6 B). In haploids or tetraploid cells, frequency of centriole disengagement was significantly lower or higher than that in diploids, respectively (Fig. 6 B). The ploidy-dependent increase in the frequency of centriole disengagement at mitotic exit was also observed in DLD-1 cells but was less prominent in RPE-1 cells (Fig. S3, E and F).

Next, we investigated the time course of the resolution of intercentriolar connection during mitotic exit using live imaging of GFP-centrin HAP1 cells with different ploidies (Fig. 6, C–E). With the spatiotemporal resolution of our imaging setting, it was difficult to unambiguously specify the exact timing of centriole disengagement. However, by quantifying the time course of intercentriolar distance during mitotic exit, we were able to follow the process of centriole separation (Fig. 6, D and E). In all ploidy states, pairs of centrioles were located within 0.6  $\mu\text{m}$  of one another at cytokinesis onset (Fig. 6 D), which approximately corresponds to the intercentriolar distance of engaged centriole pairs (Piel et al., 2000). By 30 min after cytokinesis onset, in 50% of diploid cells (6 out of 12 cells), the intercentriolar distance became  $>0.8 \mu\text{m}$  (Fig. 6 E), which approximately corresponds to that of disengaged pairs (Piel et al., 2000). In haploid cells, the progression of centriole separation was severely delayed (Fig. 6 D), and intercentriolar distance stayed below 0.8  $\mu\text{m}$  in more than 30% of these cells (4 out of 13 cells), even 140 min after cytokinesis onset (Fig. 6 E). In contrast, in tetraploid cells, the timing of centriole separation was brought forward substantially compared with that in diploids (Fig. 6, D and E). Therefore, consistent with results from the fixed-cell analysis, the efficiency of centriole separation during mitotic exit scaled with ploidy level.

To assess whether the ploidy-dependent change in the efficiency of centriole disengagement is the primary cause for the delay in centriole duplication in haploid cells, we set out to manipulate the efficiency of centriole disengagement. Previous studies have revealed that a particular fraction of pericentriolar material is involved in centriole engagement, and that the removal of a pericentriolar material component, PCNT/pericentrin/kendrin, from the centrosomes is the prerequisite for timely centriole disengagement and subsequent duplication (Lee and Rhee, 2012; Matsuo et al., 2012; Pagan et al., 2015). Therefore, we investigated the effect of PCNT depletion on the progression of centriole separation during mitotic exit in GFP-centrin haploid cells by live



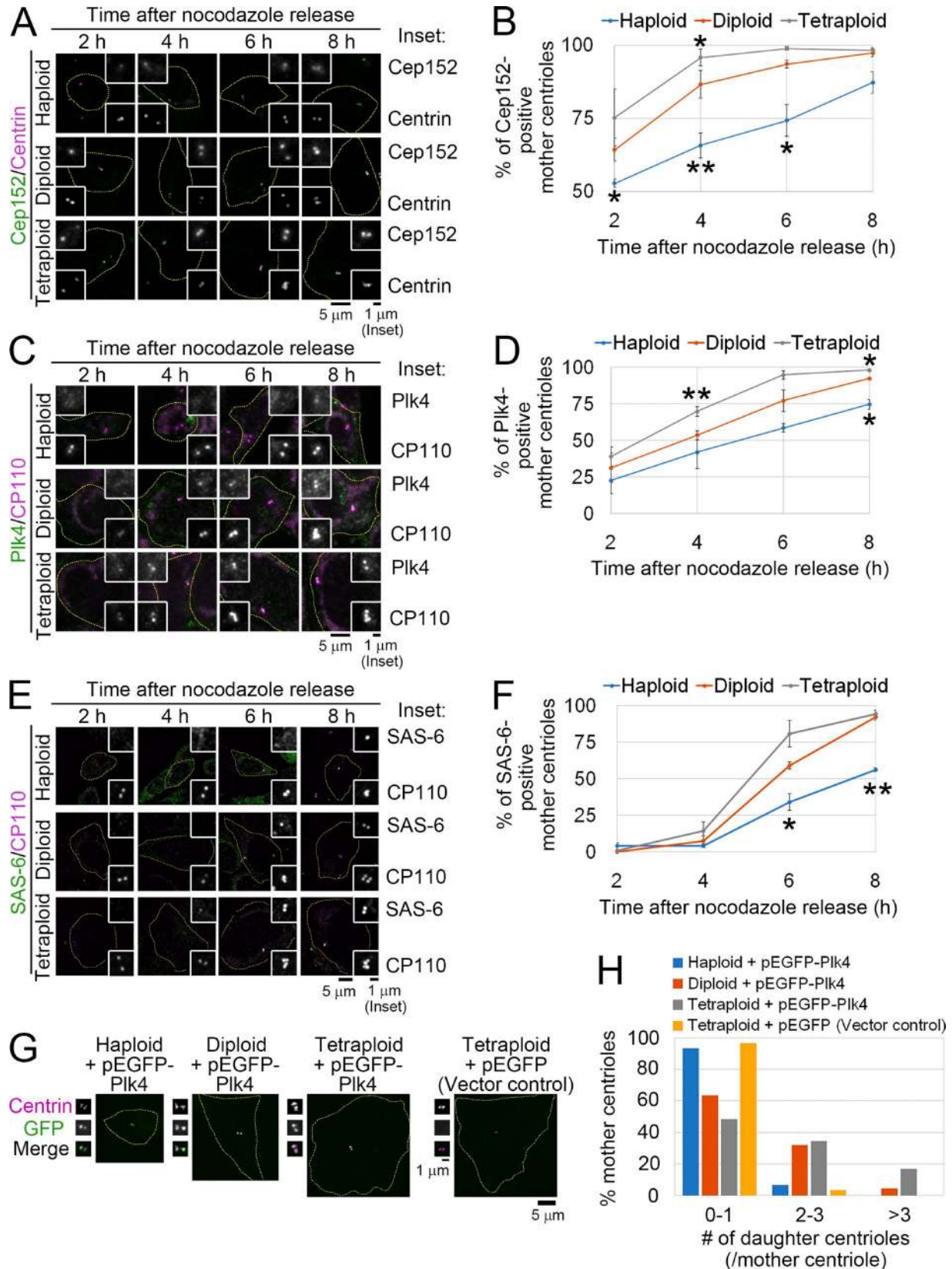


Figure 5. **Recruitment efficiency of centriole duplication factors scales to ploidy level.** (A, C, and E) Immunostaining of Cep152 (A), Plk4 (C), and SAS-6 (E) in synchronized cells with different ploidies. The centrioles were marked by immunostaining of centrin (A) or CP110 (C and E). (B, D, and F) Percentages of Cep152-, Plk4-, and SAS-6-positive mother centrioles in A, C, or E. Values represent means  $\pm$  SE of three independent experiments (asterisks indicate significant differences from diploid cells; \*,  $P < 0.05$ ; \*\*,  $P < 0.01$ ,  $t$  test). At least 114 (B), 147 (D), or 250 mother centrioles (F) were analyzed for each data point. (G) Immunostaining of centrin in HAP1 cells with different ploidies transiently expressing GFP or GFP-Plk4. Broken lines mark cell boundaries. Insets show

imaging (Fig. 7). Live imaging was conducted 48 h after RNAi treatment, when DNA content in PCNT-depleted haploid cells remained unchanged compared with that in mock-depleted haploid control cells (Fig. 7, A and B). To avoid complexity of interpretation caused by cell division defects or failure, we analyzed only the cells that successfully completed symmetric cell division without mitotic arrest. Depletion of PCNT drastically increased centriole separation efficiency in haploid cells (Fig. 7, C–E), with intercentriolar distance becoming  $>0.8 \mu\text{m}$  by 30 min in  $>70\%$  of PCNT-depleted cells (15 out of 20 cells; Fig. 7 E).

We next determined the effect of PCNT depletion on the progression of centriole duplication in haploid cells using correlative live- and fixed-cell imaging. Asynchronous mock- or PCNT-depleted HAP1 cells were live imaged from the pre- to postmitotic phase, and the progression of centriole duplication after cell division were tested by immunostaining of SAS-6 and CP110 (Fig. 8, A and B). Consistent with the result obtained in the synchronization assay (Figs. 4 C and 5 E), the progression of SAS-6 recruitment and centriole duplication in mock-depleted haploid cells was severely delayed compared with those in the diploid counterpart (Fig. 8, C and D). However, PCNT depletion considerably restored the efficiency of both the progression of SAS-6 recruitment and centriole duplication in haploid cells (Fig. 8, C and D). These results suggest that the delay in centriole disengagement is the primary cause of the delay in the progression of centriole duplication in haploid cells.

#### Ploidy-dependent difference in astral MT development determines the efficiency of centriole licensing

We next wished to understand the mechanism that changes the efficiency of centriole disengagement in a ploidy-dependent manner. Two mechanisms have been proposed to drive centriole disengagement during mitotic exit, that is, the Plk1- and separase-mediated PCNT degradation or mechanical separation of the engaged centriole pair by astral MT-driven pulling forces (Lee and Rhee, 2012; Matsuo et al., 2012; Cabral et al., 2013; Kim et al., 2015; Seo et al., 2015). Therefore, we tested whether either of these two mechanisms was affected by ploidy difference. We first tested the effect of ploidy difference on the progression of PCNT degradation during mitotic exit. To avoid any potential side effects of MT perturbation by nocodazole treatment, we arrested cells at mitotic phase using a proteasome inhibitor MG132 that blocks anaphase onset without affecting MT organization (Uetake and Sluder, 2010; Fig. S4, A and B). The degradation of PCNT after MG132 washout and mitotic shake-off progressed similarly in all ploidies, suggesting that this process was unaffected by ploidy difference. We next assessed the effect of ploidy difference on astral MT-dependent centriole disengagement. Interestingly, fluorescence microscopy of immunostained  $\alpha$ -tubulin and GFP-centrin revealed that during anaphase (when centriole separation is normally initiated), spindle poles in cells with higher ploidies developed more prominent astral MTs than those

with lower ploidies regardless of their centriole content (Fig. 9, A and B). Tracings of astral fibers revealed that the number of astral fibers associated with the cell cortex at the polar regions increased more than twofold upon doubling of ploidies (Fig. 9 B). We also compared accumulation of an essential MT organizing center factor,  $\gamma$ -tubulin, at the spindle poles among different ploidies (Fig. 9, C and D). To avoid the complexity arising from the possible influence of abnormal centriole content on  $\gamma$ -tubulin accumulation, we analyzed only the spindle poles with two centrioles. Under this analytical condition, the accumulation of  $\gamma$ -tubulin increased with ploidy levels, which possibly promotes the ploidy-dependent increase in astral MT generation. Ploidy-dependent increase in  $\gamma$ -tubulin accumulation at the spindle poles was also prominent between diploid and tetraploid DLD-1 cells, but was absent in RPE-1 cells (Fig. S3, G and H).

The poor astral MT formation in haploid cells potentially affects the efficiency of astral MT-dependent processes. Indeed, spindle tilting occurred at significantly higher frequency in haploid cells than in diploids, suggesting attenuation of astral MT function in the haploid state (Fig. S4, C and D; McNally, 2013). Therefore, to clarify the causal relationship between poor astral MT development and inefficient centriole duplication cycle in haploid cells, we next assessed whether forced enhancement of astral MTs can circumvent the delay in centriole disengagement and duplication in these cells. Previously, we observed that depletion of a spindle-associated protein complex, augmin, suppressed MT generation within the spindle and instead enhanced development of prominent astral MTs during anaphase in HeLa cells (Uehara et al., 2016). Consistent with this, when an augmin subunit, FAM29A/hDgt6/HAUS6/Aug6, was depleted by RNAi in haploid HAP1 cells, the number of astral fibers associated with the polar cortex significantly increased compared with that in control haploid cells and was similar to that in diploid cells (Fig. 9, E and F; see also Fig. 9 B). Therefore, we tested the effect of HAUS6 depletion on the progression of centriole disengagement, SAS-6 recruitment, and subsequent centriole duplication in haploid HAP1 cells (Figs. 7 and 8). At the time the experiments were conducted (2 d after siRNA transfection), a substantial population of HAUS6-depleted haploid cells remained in the haploid state, whereas mitotic arrest or cell division failure (indicated by the increase in 2C or 4C DNA content, respectively) occurred in a population because of spindle malfunctioning (Uehara et al., 2009; Fig. 7, A and B, FACS data). To avoid the potential side effects of these mitotic defects, we monitored the progression of cell division by live imaging and analyzed only cells with haploid cell size that succeeded in cell division without delay. HAUS6 depletion drastically accelerated the progression of centriole separation in haploid GFP-centrin cells (Fig. 7, C–E), and the efficiency of SAS-6 recruitment and centriole duplication in HAUS6-depleted cells was similar to that of control diploid cells in the correlative live- and fixed-cell imaging assay (Fig. 8, B–D). The

2 $\times$  (A, C, and G) or 3 $\times$  (E) enlarged images of the centrioles. (H) Quantification of daughter centrioles generated by each mother centriole in G. At least 88 mother centrioles from two (vector control) or three (others) independent experiments were analyzed for each condition. The numbers of supernumerary centrioles were significantly different between haploid and diploid or diploid and tetraploid GFP-Plk4-expressing cells ( $P < 10^{-7}$  or  $P < 0.01$ ,  $t$  test, respectively).

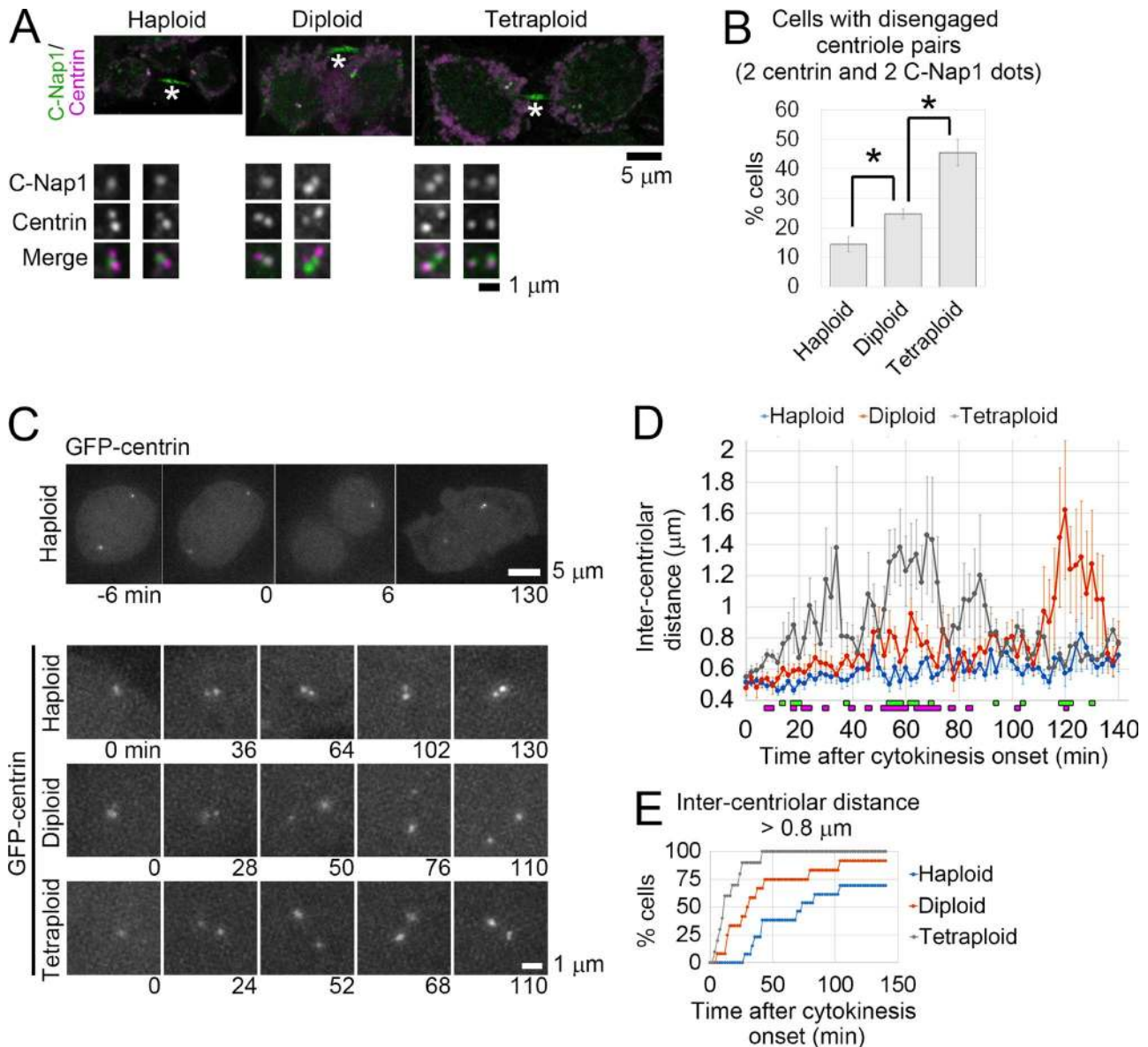


**Figure 6. The efficiency of centriole disengagement scales to ploidy level.** (A) Immunostaining of centrin and C-Nap1 in haploid, diploid, and tetraploid cells at mitotic exit. Whole-cell images (top) and 3 $\times$  enlarged images of the centrioles (bottom). Asterisks indicate nonspecific staining of the intercellular bridge. (B) Frequencies of cells with disengaged centriole pairs (with two centrin and two C-Nap1 dots) in A. Values represent means  $\pm$  SE of three independent experiments (\*,  $P < 0.05$ ,  $t$  test). At least 144 cells were analyzed for each condition. (C) Live imaging of GFP-centrin cells taken at 2-min intervals. Cytokinesis onset was set as 0 min. Whole-cell images of a haploid cell (top) and enlarged images of the centrioles in cells with different ploidy levels (bottom). (D) Time course of intercentriolar distance in C. Values represent means  $\pm$  SE of at least nine cells from at least two independent experiments for each data point (at least 10 cells were analyzed for each condition). Green or magenta markers at the bottom of the graph indicate statistically significant differences between haploid and diploid or diploid and tetraploid cells, respectively ( $P < 0.05$ ,  $t$  test). (E) Cumulative frequency of cells in which intercentriolar distance had reached 0.8  $\mu$ m in C. At least 10 cells from at least two independent experiments were analyzed for each condition.

aforementioned results indicate that the extent of astral MT development is a critical determinant of the efficiency of the centriole licensing process and subsequent centriole duplication and that inefficient centriole duplication cycle in haploid cells can be largely attributed to the poor organization of astral MTs during mitosis. Although we also wished to investigate the effect of astral MT enhancement on the stability of the haploid state, severe cell division failure and cell death caused by augmin depletion precluded us from testing its effect on haploid stability over weeks.

#### Haploid-specific centrosome loss in mouse parthenogenetic embryos

Finally, to assess whether the ploidy-linked change in centrosome homeostasis is also seen in systems other than human cultured cells, we investigated mitotic spindle organization in haploid and diploid mouse parthenogenetic embryos at embryonic day 4.5 (E4.5), a stage by which de novo centrosome generation is complete (Gueth-Hallonet et al., 1993; Latham et al., 2002; Liu et al., 2002; Courtois et al., 2012). As previously reported, morphological abnormalities were frequently observed specifically in

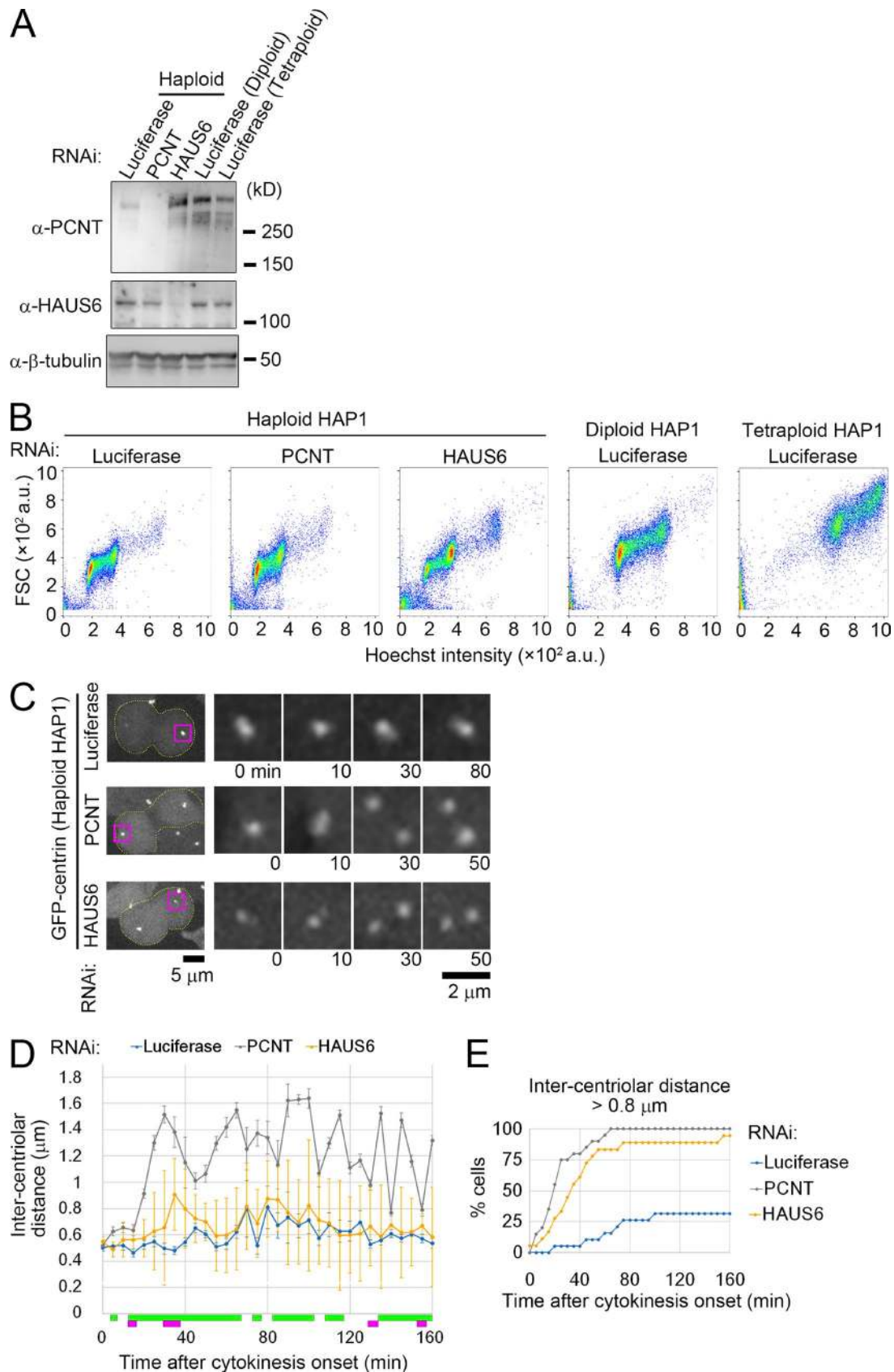


Figure 7. **Depletion of PCNT or augmin accelerates centriole separation in haploid cells.** (A) IB of PCNT, HAUS6 in RNAi-treated haploid, diploid, and tetraploid HAP1 cells.  $\beta$ -Tubulin was detected as a loading control. (B) Flow cytometric analysis of FSC and DNA content in RNAi-treated haploid, diploid, and tetraploid HAP1 cells stained by Hoechst. Representative data from two independent experiments are shown in A and B. (C) Live imaging of RNAi-treated haploid GFP-centrin cells taken at 5-min intervals. Cytokinesis onset was set as 0 min. Broken lines mark cell boundaries. Centrioles (indicated by magenta

haploid embryos (Latham et al., 2002; Liu et al., 2002; Fig. 10, A and B; and Fig. S5, A and B). A substantial proportion of mitotic cells in haploid embryos (46 out of 114 cells) had monopolar spindles with less than two centrosomes, whereas the majority of mitotic cells had bipolar spindles in diploid embryos (Fig. 10, C–E). The haploid-specific centrosome loss was also observed in embryos from another mouse strain (Fig. S5, C and D). Forced diploidization of haploid embryos through inhibition of the second cleavage at E1.5 stage fully restored the subsequent formation of normal number of centrosomes and bipolar spindles at E4.5 embryos, eliminating the possibility that the experimental procedure of haploid parthenogenesis has deleterious effects on centrosome biogenesis during the subsequent developmental stages (Fig. S5, E–G). These results suggest conservation of the ploidy-centrosome link among mammalian organisms.

## Discussion

The unstable nature of somatic haploidy in animals has been recognized for decades, but the fundamental problems in maintaining the genomic integrity of somatic cells brought about by ploidy difference are poorly understood. Through side-by-side comparison of isogenic cell lines with different ploidies, we found a linear relationship between ploidy level and efficiency of the centrosome cycle. This relationship seems to stem from the ploidy-linked scaling of astral MT development during mitosis, which promotes centriole disengagement in a ploidy-dependent manner (Fig. 10 F). This ploidy-centrosome link impairs temporal coordination between the centrosome duplication cycle and the chromosome replication cycle in non-diploid states, which would account at least in part for the relatively low tolerance of animal cells to ploidy variance compared with acentrosomal organisms such as land plants.

### Ploidy-linked scaling of centrosomal protein accumulation and astral MT development

Compared with the diploid control, haploid HAP1 cells showed severe delay in multiple key processes of the centrosome cycle such as centrosome disengagement, recruitment of duplication factors to mother centrioles, and daughter centriole formation. Because the enhancement of astral MTs by augmin depletion resolved the delay in all these processes, the poor astral MT formation appears to be the primary cause of all the observed centrosomal defects in haploid cells. In contrast, tetraploid HAP1 cells formed more robust asters than their diploid counterparts and showed up-regulation of all the above processes of the centrosome cycle, suggesting linearity of the astral MT-mediated change in centrosome duplication efficiency among different ploidies. Because  $\gamma$ -tubulin provides templates for astral MT nucleation (Oakley et al., 2015), the ploidy-linked scaling of astral MT development in HAP1 cells might result from the ploidy-dependent accumulation

of  $\gamma$ -tubulin at the spindle poles. The ploidy-dependent accumulation of  $\gamma$ -tubulin and up-regulation of centriole disengagement/duplication were also prominent in DLD-1 cells, but not in RPE-1 cells. This suggests that the ploidy-centrosome link is conserved among human cells with different tissue origins, whereas it may be absent in certain cell types. Considering the potential contribution of  $\gamma$ -tubulin to the astral MT-mediated centriole licensing process, the ploidy dependency of the centrosome cycle in specific cell types may be determined by the presence or absence of the ploidy-dependent scaling of  $\gamma$ -tubulin accumulation at the mitotic centrosomes. However, the determinants of ploidy dependent accumulation of  $\gamma$ -tubulin in different cell types remain unknown. In early *Caenorhabditis elegans* embryos, centrosome size gradually decreases with progress of the cell division cycle because of the reduction in cell size and the available pool of centrosomal proteins (Decker et al., 2011). Similar centrosome scaling may occur if protein production and/or cell size drastically changes upon ploidy conversion. Indeed, we observed that the levels of total protein or several centrosomal proteins per cell, as well as cell size, increased proportionally with ploidy level (Fig. S1 C; and Fig. S4, E–H). However, because the ploidy-dependent increase in centrosomal protein was also observed in RPE-1 cells, another unidentified layer of regulation that determines ploidy dependency of centrosomal protein accumulation in different cell types might exist.

Besides centrosomal protein accumulation at the spindle poles during mitosis, the accumulation of some key centriole duplication factors, such as Cep152 and Plk4, also changed in a ploidy-dependent manner during G1/S phase. The general reduction in the amounts of centriole duplication factors at the centrosomes potentially endangers centrosome homeostasis in haploid states, especially considering that some important duplication factors such as Plk4 or NDC1 in yeast cells show haploinsufficiency (Chial et al., 1999; Ko et al., 2005). However, we found that augmin depletion singly restored the efficiency of SAS-6 recruitment and centriole duplication in haploid cells. These results indicate that that single-gene copies of centriole duplication factors are sufficient to support the normal progression of centriole duplication in a haploid background. However, we cannot rule out the possibility that ploidy-dependent accumulation of centriole duplication factors influences the efficiency of centriole duplication in hyperploidy states. It is also important that future studies examine whether ploidy-dependent changes in centrosomal protein enrichment have any influence on the ultrastructure of the centriole throughout the centrosome duplication cycle.

### Generality of the ploidy-centrosome link among animal organisms

Although the ploidy-centrosome link seems preserved between human cultured cells and mouse embryonic cells, it remains to

boxes) are enlarged in the right panels. (D) Time course of intercentriolar distance in C. Values represent means  $\pm$  SE of at least 14 cells from two independent experiments for each data point (at least 18 cells were analyzed for each condition). Green or magenta markers at the bottom of the graph indicate statistically significant differences between mock-depleted and PCNT-depleted, or HAUS6-depleted haploid cells, respectively ( $P < 0.05$ ,  $t$  test). (E) Cumulative frequency of cells in which intercentriolar distance had reached 0.8  $\mu$ m in C. At least 18 cells from two independent experiments were analyzed for each condition.

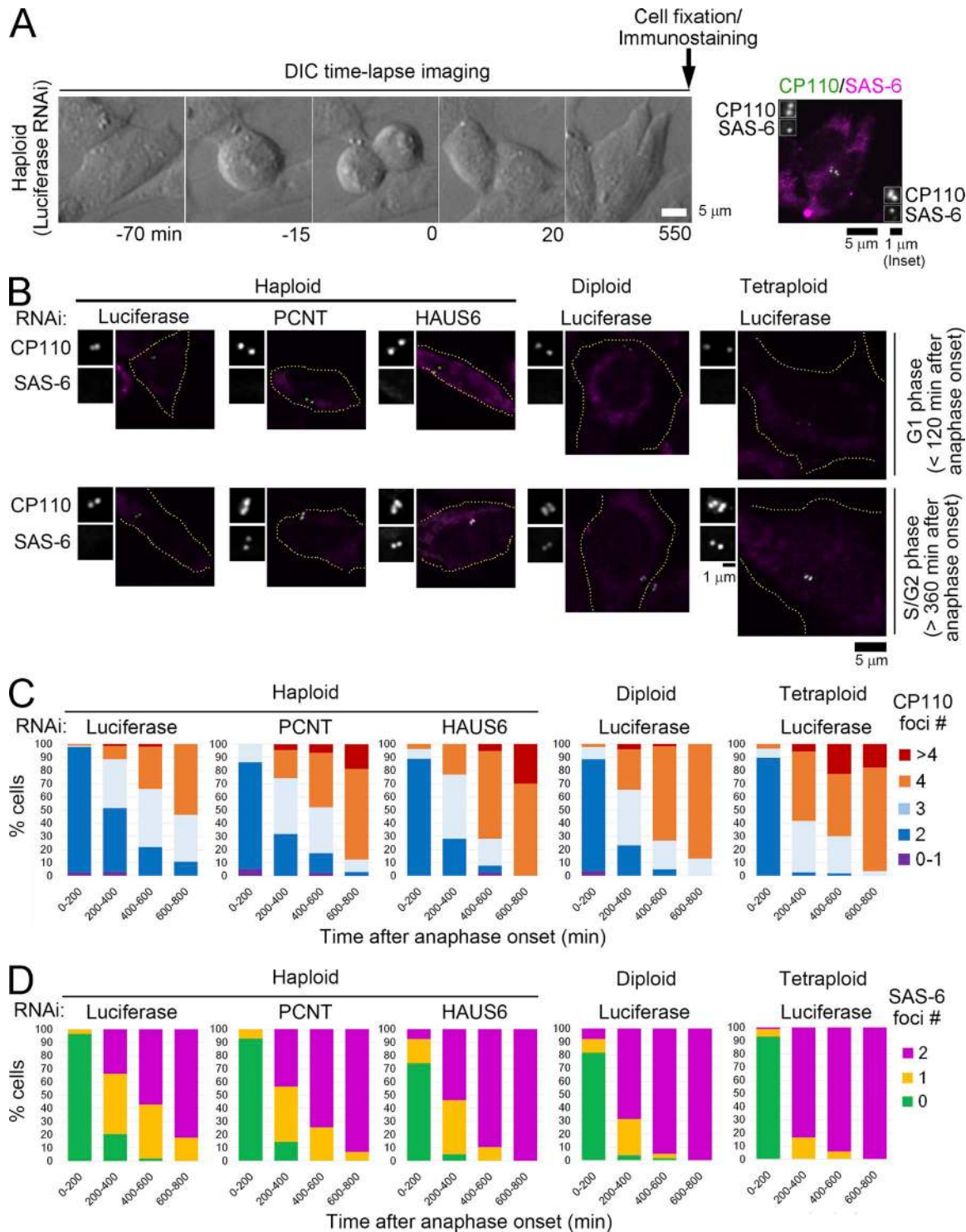


Figure 8. **Depletion of PCNT or augmin accelerates centriole duplication in haploid cells.** (A) Correlative live- and fixed-cell imaging. RNAi-treated HAP1 cells were live imaged by DIC microscopy every 5 min for 16 h (left) and then fixed and subjected to immunostaining against CP110 and SAS-6. The cells that passed the mitotic phase during time-lapse imaging were identified using grid patterns on the culture dish and observed using fluorescence microscopy (right). Anaphase onset was set as 0 min. (B) Immunostaining of CP110 and SAS-6 in RNAi-treated HAP1 cells in the correlative live and fixed cell imaging. Insets show 2 $\times$  enlarged images of the centrioles in A and B. Broken lines mark cell boundaries. (C and D) Percentages of cells with indicated numbers of CP110 foci (C) or SAS-6 foci (D) at each time window after anaphase onset in B. At least 114 cells from two independent experiments were analyzed for each condition (at least 10 cells for each data point). Note that percentage of the cells that possessed three or four centriole foci increased in PCNT- or HAUS6-depleted haploid cells compared with control haploid cells in a 200- to 400-min time window, indicating that the initiation of centriole duplication was accelerated in these cells.

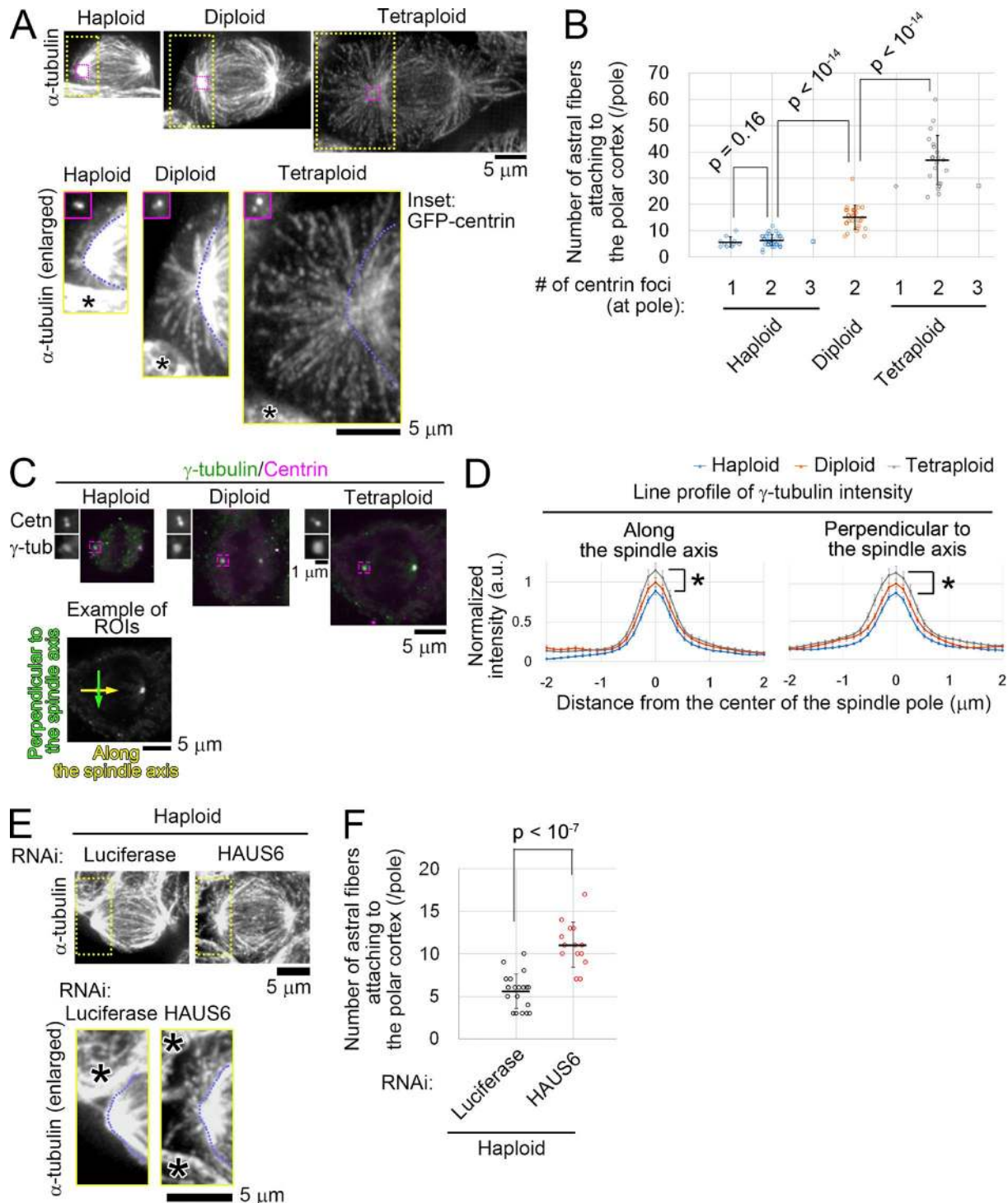


Figure 9. **Development of astral MTs scales to ploidy level. (A and E)** Immunostaining of  $\alpha$ -tubulin during anaphase in GFP-centrin HAP1 cells with different ploidies (A) or in RNAi-treated haploid HAP1 cells (E). Enlarged images of the astral MTs at the polar region (yellow boxes) and GFP-centrin at the spindle pole (magenta boxes in A) are shown in the bottom panels. Asterisks: neighboring interphase cells. Blue broken lines: spindle regions. **(B and F)** Number of astral fibers attached to the polar cortex in A or E. Values represent means  $\pm$  SD of at least 10 spindle poles from three independent experiments (B) or at least 14 poles from two independent experiments (F;  $p$ -values calculated using  $t$  tests are shown). Spindle poles with different numbers of GFP-centrin foci were separately categorized in B. Examples of MT tracking are shown in Video 7. **(C)** Immunostaining of  $\gamma$ -tubulin and centrin in preanaphase cells with different ploidies. Insets show 2 $\times$  enlarged images of the spindle poles indicated by magenta boxes. Bottom: An example of regions of interest (ROIs) for the quantification in D. **(D)** Line profiles of  $\gamma$ -tubulin at the spindle poles in C. Spindle poles with two centrioles were analyzed. Values represent means  $\pm$  SE of at least 24 spindle poles from two independent experiments. Asterisks indicate statistically significant differences between haploid and tetraploid cells at the center of the spindle pole (\*,  $P < 0.05$ , one-way ANOVA with Tukey post-hoc test).

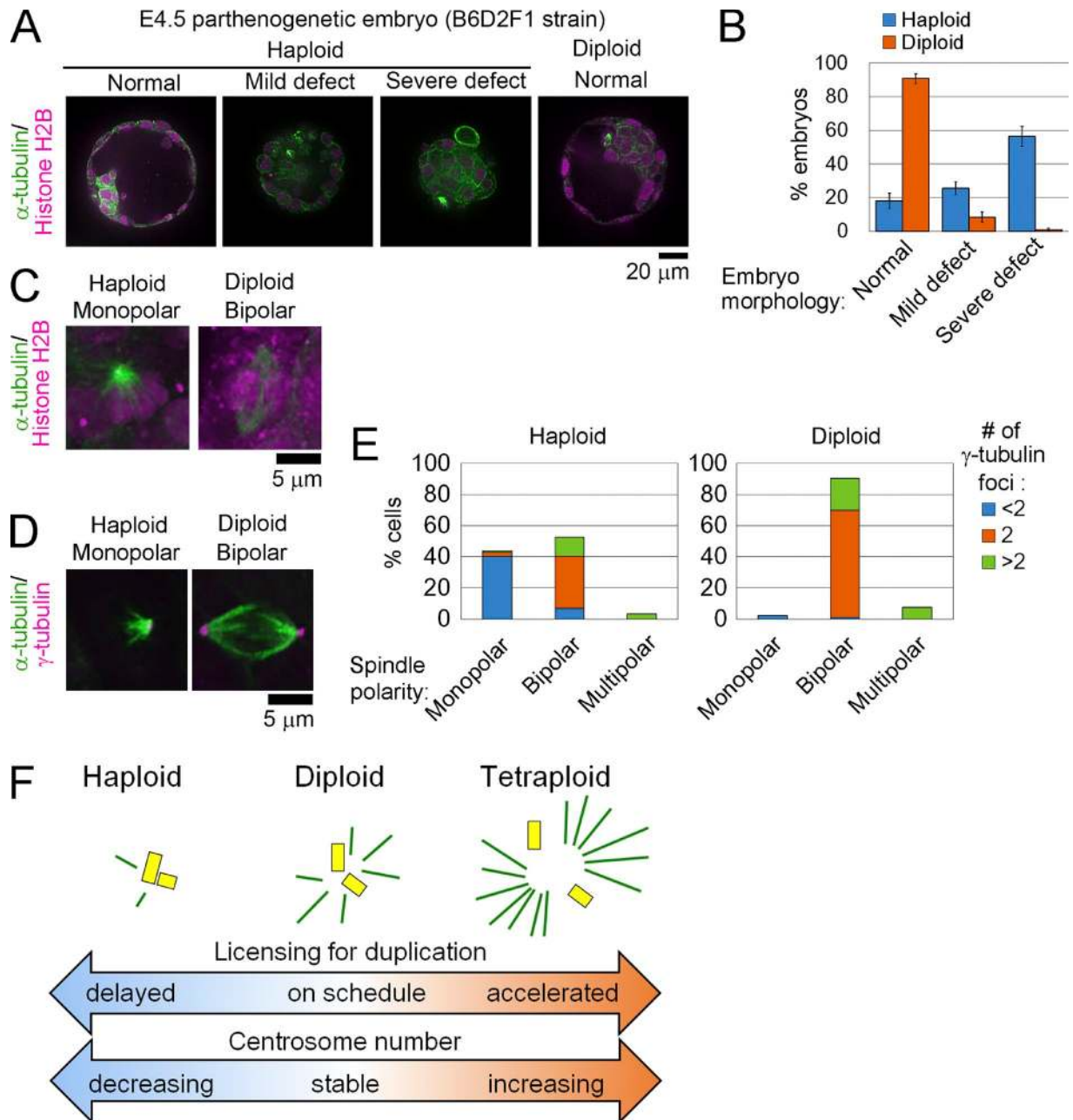


Figure 10. **Centrosome reduction and monopolar spindle formation in haploid mouse embryos.** (A, C, and D) Immunostaining of  $\alpha$ -tubulin and histone H2B (A and C), or  $\gamma$ -tubulin (D) in B6D2F1 mouse parthenogenetic embryos at E4.5. Mitotic cells are shown in C and D. (B) Frequencies of morphological abnormalities in A. Values represent means  $\pm$  SE of four independent experiments. At least 109 embryos were analyzed per condition. (E) Spindle polarities and numbers of  $\gamma$ -tubulin foci in D. At least 93 cells from 71 embryos from 11 independent experiments were analyzed per condition. (F) A model for the ploidy-centrosome link. During mitosis, astral MTs (lines) develop in a ploidy-linked manner. Inadequate or excess amounts of asters lead to deceleration or acceleration of centriole disengagement (and subsequent duplication), respectively, in haploid or tetraploid cells, respectively. As a result, the efficiency of the entire centriole duplication cycle scales proportionally to ploidy level, which drives uncoupling of centriole duplication and DNA replication in non-diploid states.

be elucidated whether it is also conserved among nonmammalian animal species. Of interest, however, is that in different fish species, haploid embryos develop abnormally small brains and eyes (Araki et al., 2001; Patton and Zon, 2001; Luo and Li, 2003), which are very similar to morphological defects reported in zebrafish embryos depleted of several centrosomal genes (Kim et al., 2011; Novorol et al., 2013). Therefore, it is intriguing to speculate that these developmental defects observed in haploid fishes

are caused by haploidy-driven centrosome loss. Another hint on the generality of the ploidy-centrosome link is that cell lines derived from haploid lethal embryos of a *Drosophila melanogaster* mutant are devoid of centrioles (Debec, 1978, 1984; Szöllösi et al., 1986; Debec and Abbadié, 1989). Although in the original articles, the centrosome loss in these cell lines was attributed to an unidentified mutation in the original embryos, it is also possible that their haploid state by itself drove the centrosome



loss. Further analyses using nonmammalian organisms would improve our understanding of the general impact of ploidy difference on centrosome homeostasis.

### Attenuation of centrosome-independent pathway in haploid cells

Our results indicate that the frequent mitotic failure in haploid cells and subsequent diploidization are caused by combinational effect of haploidy-linked centrosome loss and attenuation of the centrosome-independent pathway. Currently, the reason behind the poor efficiency of centrosome-independent spindle formation in the haploid state is not known. However, as chromosome number potentially affects Ran-GTP gradient formation (Hasegawa et al., 2013), the lesser number of chromosomes in haploid cells may attenuate the Ran-GTP-dependent pathway and suppress centrosome-independent spindle formation. Ran-GTP may also be involved in ploidy-linked scaling of mitotic centrosomes through its downstream factors involved in centrosome maturation (Petretti et al., 2006; Yokoyama et al., 2008).

### Potential importance of the hyperploidy-driven centriole overduplication

The ploidy-dependent up-regulation of centriole duplication suggests a new route to centrosome amplification in hyperploidy tumor cells. Hyperploidy tumor cells often possess extra centrosomes, which conceivably arise from cell division failure in ancestor cells (Godinho and Pellman, 2014). The extra centrosomes are normally purged from the progeny cell population because of the disadvantages associated with multipolar spindle formation, but they are sustained in some populations through an adaptation mechanism that promotes centrosome clustering or selection owing to their invasive qualities (Ganem et al., 2009; Godinho et al., 2014; Rhys et al., 2018). In addition to these mechanisms, the hyperploidy state itself may promote chronic deregulation of centrosome number control as observed in HAP1 or DLD-1 cells and thus may contribute significantly to the maintenance of extra centrosomes in hyperploidy tumor cells. Future investigations on the contribution of hyperploidy-driven centrosome overduplication to genome instability during cancer development using *in vivo* models are required.

## Materials and methods

### Cell culture and flow cytometry

The HAP1 cell line (Haplogen) was cultured in Iscove's modified Dulbecco's medium (IMDM; Wako) or DMEM (Wako; for cell viability assay) supplemented with 10% FBS and 1× antibiotic-antimycotic (1× AA; Sigma-Aldrich) on culture dishes coated with rat tail type-I collagen (Corning). hTERT-RPE-1, DLD-1, and HeLa cell lines were cultured in DMEM supplemented with 10% FBS and 1× AA. Haploid HAP1 cells were purified by sorting based on forward scatter (FSC) intensity using a JSAN desktop cell sorter (Bay bioscience). For each sorting,  $\sim 10^6$  cells were collected. Sorted cells were cultured for a further 6–7 d to reach subconfluence on 15-cm dishes (Nippon Genetics) and then stored in freezing medium (Bambanker; Lymphotec) as 5–6 aliquots in vials (Corning) at  $-80^{\circ}\text{C}$  or  $-196^{\circ}\text{C}$ . Every cell culture lot was checked for

DNA content as described below. Haploid-enriched cells were used within 7 d after recovery from frozen stocks for all experiments to minimize the effects of spontaneous diploidization. For long-term culture experiments, the point at which haploid-enriched HAP1 cell stocks were freshly thawed was set as “day 0,” and cells were cultured for several weeks, with passaging every 1–3 d. To obtain diploid HAP1 cells, haploid-enriched cells were cultured for a few weeks, and the spontaneously diploidized cell population purified by FSC-based sorting. To obtain tetraploid HAP1 or DLD-1 cells, diploid cells were treated with  $2.5\ \mu\text{M}$  cytochalasin D for 16 h to induce cytokinesis failure, washed three times with cell culture medium, and then subjected to limiting dilution. After 10 d, colonies containing cells that were uniform in size and larger than diploid cells were picked and cultured, and their ploidy states were tested by DNA content analyses using flow cytometry to select tetraploid clones. To obtain tetraploid RPE-1 cells, cytokinesis failure was induced in diploid cells as described above, and the tetraploidized cell population was purified by sequential cell sorting based on Hoechst 33342 signal intensities. The HAP1 EGFP- $\alpha$ -tubulin or GFP-centrin cell line was established by transfecting HAP1 cells with pEGFP- $\alpha$ -tubulin vector (Uehara and Goshima, 2010) or pEGFP-centrin2 vector (Kleylein-Sohn et al., 2007; plasmid 41147; Addgene), respectively, and selecting positive cells that grew in the presence of  $500\ \mu\text{g}/\text{ml}$  G418 (Wako). For DNA content analyses, cells were cultured until they reached subconfluence on 10-cm dishes and then trypsinized, washed once with Dulbecco's PBS (DPBS; Wako), suspended in 1 ml DPBS at a density of  $2 \times 10^6$  cells/ml, stained with  $10\ \mu\text{g}/\text{ml}$  Hoechst 33342 (Dojindo) for 15 min at  $37^{\circ}\text{C}$ , and washed once with DPBS, and their DNA content was analyzed using a JSAN desktop cell sorter. In each DNA content analysis,  $2 \times 10^4$  cells were counted. For viability assay of centrinone B-treated cells, the cell counting kit-8 (CCK-8; Dojindo) was used following the manufacturer's instructions. Absorbance of each well at 450 nm was measured using the Sunrise plate reader (Tecan).

### RNAi

For siRNA transfection, Lipofectamine RNAiMAX (Thermo Fisher Scientific) was used following the manufacturer's instructions. The siRNAs used in this study were 5'-CGUACGCGAAUACUUCGATT-3' (luciferase), 5'-CAGUUAAGCAGGUACGAAATT-3' (HAUS6; Uehara et al., 2009), and 5'-UGGACGCUAUCCAAUGAGATT-3' (PCNT; Kim et al., 2015). Cells were subjected to live cell imaging or flow cytometry analyses 48 h after siRNA transfection.

### Immunofluorescence (IF) staining

For IF staining of centrosomal proteins and mitotic spindles, cells or embryos were fixed with 100% methanol at  $-20^{\circ}\text{C}$  for 10 min. For IF of astral MTs, cells were fixed with 3.2% PFA and 2% sucrose in DPBS for 10 min at  $37^{\circ}\text{C}$  and permeabilized with 0.5% Triton X-100 in DPBS supplemented with 100 mM glycine (DPBS-G) on ice for 5 min. For IF of incorporated BrdU, cells were prefixed with 100% methanol at  $-20^{\circ}\text{C}$  for 10 min, postfixated with 3.7% PFA in DPBS for 15 min at  $25^{\circ}\text{C}$ , and treated with 1% Triton X-100 in 4 N HCl for 5 min at  $25^{\circ}\text{C}$ . Fixed samples were treated with BSA blocking buffer (150 mM NaCl, 10 mM Tris-HCl, pH

7.5, 5% BSA, and 0.1% Tween 20) for 30 min at 25°C, incubated with primary antibodies overnight at 4°C, and incubated with secondary antibodies for 1 h at 37°C or overnight at 4°C. After each treatment, cells were washed two to three times with DPBS or DPBS-G. Stained cells were mounted with mounting medium (90% [vol/vol] glycerol; 100 mM Tris-HCl, pH 8.0, and 0.5% [wt/vol] *N*-propyl gallate). Stained mouse embryos were embedded in 0.5% PrimeGel Agarose LMT (Takara Bio) dissolved in DPBS.

### SDS-PAGE and immunoblotting (IB)

For SDS-PAGE, cells were lysed in SDS-PAGE sample buffer, and boiled for 5 min. For quantification of the total protein amount per cell, aliquots of cell lysate corresponding to  $2.5\text{--}5 \times 10^4$  cells were loaded into each well of gels. Separated proteins were stained using Coomassie brilliant blue, and the total protein amount in each lane quantified using BSA as a standard. For IB, proteins separated by SDS-PAGE were transferred to Immun-Blot PVDF membrane (Bio-Rad). Membranes were then blocked with 0.3% skim milk in TTBS (50 mM Tris, 138 mM NaCl, 2.7 mM KCl, and 0.1% Tween 20) incubated with primary antibodies overnight at 4°C or for 1 h at 37°C and with secondary antibodies for 30 min at 37°C. Each step was followed by three washes with TTBS. Signal detection used the ezWestLumi plus ECL Substrate (ATTO) and a LuminoGraph II chemiluminescent imaging system (ATTO).

### Antibodies

Antibodies were purchased from suppliers and used at the following dilutions: rat monoclonal anti- $\alpha$ -tubulin (1:1,000 for IF and 1:500 for IB; YOL1/34; EMD Millipore); mouse monoclonal anti- $\beta$ -tubulin (1:1,000 for IB; 10G10; Wako); goat polyclonal anti-Histone H2B (1:50 for IF; sc-8650; Santa Cruz Biotechnology); mouse monoclonal anti-centrin (1:1,000 for IF and 1:200 for IB; 20H5; EMD Millipore); rabbit polyclonal anti-centrin 2 (1:50 for IF; sc-27793; Santa Cruz Biotechnology); mouse monoclonal anti- $\gamma$ -tubulin (1:200 or 1:100 for IF in HAP1 cells, 1:100 for IF in mouse embryos, and 1:1,000 for IB; GTU88; Sigma-Aldrich); rabbit polyclonal anti-Cep152 (1:1,000 for IF and 1:500 for IB; ab183911; Abcam); mouse monoclonal anti-Plk4 (1:500 for IF; 6H5; EMD Millipore); rabbit polyclonal anti-CPI10 (1:500 for IF; A301-343A; Bethyl Laboratories); mouse monoclonal anti-SAS-6 (1:50 for IF and 1:200 for IB; sc-81431; Santa Cruz Biotechnology); rabbit polyclonal anti-C-Nap1 (1:200 for IF; 14498-1-AP; Proteintech); rabbit polyclonal anti-PCNT (1:200 for IB; ab4448; Abcam); rabbit polyclonal anti-hDgt6/HAUS6 (1:500 for IB; Uehara et al., 2009); rat monoclonal anti-BrdU (1:50 for IF; sc-56258; Santa Cruz Biotechnology); and fluorescence (Alexa Fluor 488, Rhodamine Red-X, or Alexa Fluor 594) or horseradish peroxidase-conjugated secondaries (1:1,000 for IF and IB; Jackson ImmunoResearch Laboratories).

### Microscopy

Fixed or living cells were observed at 25°C or 37°C with 5% CO<sub>2</sub>, respectively, under a TE2000 microscope (Nikon) equipped with a 100 $\times$  1.4 NA Plan-Apochromatic, a 60 $\times$  1.4 NA Plan-Apochromatic, or a 40 $\times$  1.3 NA Plan Fluor oil immersion objective lens (Nikon), a CSU-X1 confocal unit (Yokogawa), and an iXon3 electron multiplier-charge-coupled device camera (Andor) or an ORCA-ER CCD camera (Hamamatsu Photonics). Image acquisition was controlled

by  $\mu$ Manager software (Open Imaging). Long-term live imaging for cell cycle analyses was performed using a LCV110 microscope (Olympus) equipped with a 40 $\times$  0.95 NA UPLSAPO dry lens (Olympus). Because we found that 488-nm light irradiation severely interfered the progression of cell cycle and mitosis in HAP1 cells, we used bright-field microscope for long-term live imaging for cell cycle analyses (Figs. 1, 8, and S3). For live imaging, cells were cultured in phenol red-free IMDM (Thermo Fisher Scientific) supplemented with 10% FBS and 1 $\times$  AA.

### Cell cycle synchronization

Asynchronous HAP1 cell cultures were treated with 20 ng/ml nocodazole (Wako) for 4 h or with 3  $\mu$ M MG132 (Peptide Institute) for 1 h and then washed with IMDM supplemented with 10% FBS and 1 $\times$  AA three times. Mitotic cells were dislodged from the culture dishes by tapping and then transferred to collagen-coated 8-well coverglass chambers (Zelkontakt) or 6-well dishes (Nippon Genetics) and synchronized cells sampled at each time point indicated. To arrest cells in early S phase, the nocodazole-released cells were treated with 4 mM thymidine (Wako).

### Correlative live- and fixed-cell imaging

To compare the progression of centriole duplication and SAS-6 recruitment among isogenic cells with different ploidy in asynchronous culture condition, cells were cultured on dishes with grid patterns (AGC Techno Glass), subjected to differential interference contrast (DIC) time-lapse imaging for 16–24 h to identify the cells that passed the mitotic phase. Cells were then fixed and subjected to immunostaining against centrin and SAS-6 to quantify centriole number in the live-monitored cells that were identified by grid patterns on the dishes. By quantifying the distribution of centriole numbers in respective time windows after mitotic exit, we were able to monitor and compare the progression of centriole duplication among cells with different ploidy or with different RNAi conditions.

### Exogenous expression of GFP-Plk4 in HAP1 cells

Full-length cDNA of human Plk4 (GenBank accession no. [NM014264.4](#)) was obtained from the RPE-1 cell cDNA pool by PCR using primers 5'-ATCTCGAGCACCATGGCGACCTGCATCGGGGAGAAG-3', and 5'-ATGGATCCCGATGAAAATTAGGAGTCGATTAG-3', and subcloned into the XhoI and BamHI sites of pEGFP-C1 (Takara Bio). Mitotic cells were collected by shake-off, transfected with the plasmid using Nucleofector 2b (Lonza), and then arrested in the early S phase by 16-h thymidine treatment. Centriole overduplication was monitored by centrin immunostaining. Under this condition, the overduplicated daughter centrioles were connected to their mother centrioles, enabling the quantification of daughter centriole generated from each mother centriole (Habedanck et al., 2005).

### Theoretical modeling of the progression of diploidization

To theoretically assess the impact of haploid-specific mitotic defects and cell cycle delay on the stability of the haploid state in HAP1 cells, we constructed a mathematical model based on the following simple assumptions: (1) haploid and diploid populations proliferate exponentially with characteristic doubling times

corresponding to their cell cycle lengths (Fig. 1 D); (2) haploid cells die or convert into diploids through mitotic death or mitotic slippage, respectively, with the observed frequencies (Fig. 1 F); and (3) the proportion of cells in G1 phase remains unchanged in haploid populations throughout long-term culture. The basic time-dependent growth of a cell population can be modeled as

$$N(t) = 2^{\frac{t}{\tau}} \times N(0),$$

where  $N$  is the number of cells at time point,  $t$ , and  $\tau$  is the mean cell cycle length in the cell population.

Assuming ergodicity in the processes of the cell cycle, mitosis, and cell proliferation, the probability of the occurrence of mitotic death in a haploid cell population during unit time length,  $p_{death}$ , is derived as

$$p_{death} = \frac{q_{death}}{\tau_{haploid}},$$

and mitotic slippage in a haploid cell population during unit time length,  $p_{slippage}$ , as

$$p_{slippage} = \frac{q_{slippage}}{\tau_{haploid}},$$

where  $q_{slippage}$  and  $q_{death}$  are the rate of incidence of mitotic slippage and mitotic death per mitotic event, respectively, and  $\tau_{haploid}$  is the mean cell cycle length of a haploid cell population. The time-dependent growth of a haploid cell population is then modeled as

$$N_{haploid}(t) = [2(1 - p_{slippage} - p_{death})]^{\frac{t}{\tau_{haploid}}} \times N_{haploid}(0),$$

where  $N_{haploid}$  is the number of haploid cells at the time point,  $t$ . A haploid cell that converts to diploid through mitotic slippage at any point during the simulation will thereafter proliferate with the characteristic doubling time of diploid cells. The time-dependent growth of a diploid cell population is, therefore, modeled as

$$N_{diploid}(t) = 2^{\frac{t}{\tau_{diploid}}} \times N_{diploid}(0) + \sum_{i=1}^t 2^{\frac{t-i}{\tau_{diploid}}} \times N_{haploid}(i-1) \times p_{slippage},$$

where  $N_{diploid}$  is the number of diploid cells at time point,  $t$ , and  $\tau_{diploid}$  is the mean cell cycle length of a diploid cell population. Finally, the time-dependent change in the percentage of haploid cells in G1,  $P_{haploid,G1}$ , in a cell culture is modeled as

$$P_{haploid,G1} = F_{haploid,G1} \times \left( \frac{100 \times N_{haploid}}{N_{haploid} + N_{diploid}} \right),$$

where  $F_{haploid,G1}$  is the fraction of cells in G1 phase within a haploid cell population.

Computer programs were written using MATLAB (MathWorks). Parameters used in simulations are listed in Table S1.

### Image analyses

To estimate the sizes of HAP1 cells with different ploidy levels, the areas of trypsinized round-shaped cells were measured using the ROI tool in ImageJ software (National Institutes of Health), and the cell radius,  $r$ , was calculated using the equation  $r = \sqrt{A/\pi}$ , where  $A$  is the measured cell area.

The fluorescence intensities of centrosome-associated IF signals were measured using plot profile or round-shaped ROIs with diameters of 0.53  $\mu\text{m}$  (ImageJ), with subtraction of

background signals in the areas outside the cells or the cytoplasmic areas, respectively. Measurement of intercentriolar distance in GFP-centrin cells or counting of astral fibers in fixed anaphase cells was performed using the Line tool or the Manual tracking tool in ImageJ, respectively.

### Statistical analysis

Analyses for significant differences between two groups were conducted using the one-tailed Student's  $t$  test in Excel software (Microsoft). Multiple group analysis in Fig. 9 D was conducted using the one-way ANOVA with Tukey post-hoc test in R software (The R Foundation). Statistical significance was set at  $P < 0.05$ .  $p$ -values are indicated in figures or the corresponding figure legends. Data distribution was assumed to be normal, but this was not formally tested. The plus/minus sign in the main text indicates standard deviation.

### Parthenogenesis and embryo culture

C57BL/6 and DBA/2 mice were purchased from Japan SLC, and CBA mice were from Charles River Laboratories Japan. For mouse embryo experiments, 8- to 12-wk-old female B6D2F1 (C57BL/6  $\times$  DBA/2) or BCF1 mice (C57BL/6  $\times$  CBA) were injected with 5 IU pregnant mare serum gonadotropin (ASKA Animal Health) followed by injection with 5 IU human chorionic gonadotropin (ASKA Pharmaceutical) 46–48 h later, and matured oocytes were obtained from oviducts 16 h later. Haploid and diploid parthenogenetic embryos were produced as described previously, with slight modifications (Latham et al., 2002; Kishigami and Wakayama, 2007). Oocytes were treated with 0.1% hyaluronidase (Sigma-Aldrich) in M2 medium (Sigma-Aldrich) for 30 s to remove cumulus cells, washed with M2 medium and M16 medium (Sigma-Aldrich) three times each, and incubated in M16 medium supplemented with 2 mM EGTA (EGTA-M16) for 20 min. To produce haploid parthenogenetic embryos, these oocytes were treated with 5 mM SrCl<sub>2</sub> in EGTA-M16 for 2.5 h. Diploid parthenogenetic embryos were produced by treating the oocytes with 5 mM SrCl<sub>2</sub> in EGTA-M16 in the presence of 5  $\mu\text{g}/\text{ml}$  cytochalasin B (Wako) for 2.5 h and then incubating them in KSOM medium (MTI-GlobalStem) in the presence of the same concentration of cytochalasin B for 3.5 h. Activated haploid and diploid parthenogenetic embryos were then washed with KSOM three times and cultured in the same medium at 37°C with 5% CO<sub>2</sub>. In case haploid embryos were converted to diploid after parthenogenesis, E1.5 embryos were treated with 5  $\mu\text{g}/\text{ml}$  cytochalasin B for 12 h to block the second cleavage and washed three times with KSOM.

### Ethics statement

The maintenance and handling of mice for all embryo experiments were performed in the animal facility of the Platform for Research on Biofunctional Molecules of Hokkaido University under the guidelines and with the permission of the committee on animal experiments of Hokkaido University (permission number 16-0038).

### Online supplemental material

Fig. S1 shows additional analyses of isogenic HAP1 cells with different ploidies. Fig. S2 shows ploidy-dependent changes in

centriole duplication in HAP1 cells. Fig. S3 shows ploidy-dependent changes in centrosome cycle in RPE-1 and DLD-1 cells. Fig. S4 shows comparison of PCNT degradation, spindle positioning, and protein expression among different ploidy states. Fig. S5 shows additional data on centrosome loss in haploid mouse embryos. Table S1 shows parameters used in the simulation. Source code files used in the simulation for modeling dynamics of haploid cell population (haploid.txt) and for drawing plots (plot\_hap.txt) are also provided.

## Acknowledgments

We are grateful to M. Mishra, S. Bulchand, T. Kamasaki, and G. Goshima for valuable comments on the draft of this paper, M.F. Tsou for GFP-centrin live imaging advice, and the members of the Faculty of Advanced Life Science and the Open Facility (Hokkaido University) for the use of their equipment.

This work was supported by the Akiyama Life Science Foundation, the Inamori Foundation, the Mochida Memorial Foundation, the Naito Foundation, the Nakajima Foundation, the Noastec Foundation (grant T-3-9), the SGH Foundation, the Suhara Memorial Foundation, the Sumitomo Foundation (grant 150105), the Takeda Science Foundation, the Uehara Memorial Foundation (grant G15118), and Ministry of Education, Culture, Sports, Science and Technology-Japan/Japan Society for the Promotion of Science KAKENHI (grants 15K14501 and 17K15111) to R. Uehara.

The authors declare no competing financial interests.

Author contributions: Conceptualization, K. Yaguchi, and R. Uehara; Methodology, K. Yaguchi, T. Yamamoto, R. Matsui, A. Shibamura, K. Kamimura, T. Koda, and R. Uehara; Software, T. Yamamoto, R. Matsui, Y. Tsukada, and R. Uehara; Investigation, K. Yaguchi, T. Yamamoto, R. Matsui, and R. Uehara; Formal Analysis, K. Yaguchi, T. Yamamoto, R. Matsui, and R. Uehara; Resources, T. Koda, and R. Uehara; Writing – Original Draft, R. Uehara; Writing – Review & Editing, Y. Tsukada, T. Koda, and R. Uehara; Funding Acquisition, T. Koda, and R. Uehara.

Submitted: 29 January 2017

Revised: 27 September 2017

Accepted: 9 April 2018

## References

Araki, K., H. Okamoto, A.C. Graveson, I. Nakayama, and H. Nagoya. 2001. Analysis of haploid development based on expression patterns of developmental genes in the medaka *Oryzias latipes*. *Dev. Growth Differ.* 43:591–599. <https://doi.org/10.1046/j.1440-169X.2001.00601.x>

Bettencourt-Dias, M., A. Rodrigues-Martins, L. Carpenter, M. Riparbelli, L. Lehmann, M.K. Gatt, N. Carmo, F. Balloux, G. Callaini, and D.M. Glover. 2005. SAK/PLK4 is required for centriole duplication and flagella development. *Curr. Biol.* 15:2199–2207. <https://doi.org/10.1016/j.cub.2005.11.042>

Cabral, G., S.S. Sans, C.R. Cowan, and A. Dammermann. 2013. Multiple mechanisms contribute to centriole separation in *C. elegans*. *Curr. Biol.* 23:1380–1387. <https://doi.org/10.1016/j.cub.2013.06.043>

Carette, J.E., M. Raaben, A.C. Wong, A.S. Herbert, G. Obernosterer, N. Mulherkar, A.I. Kuehne, P.J. Kranzusch, A.M. Griffin, G. Ruthel, et al. 2011. Ebola virus entry requires the cholesterol transporter Niemann-Pick C1. *Nature.* 477:340–343. <https://doi.org/10.1038/nature10348>

Chial, H.J., T.H. Giddings Jr., E.A. Siewert, M.A. Hoyt, and M. Winey. 1999. Altered dosage of the *Saccharomyces cerevisiae* spindle pole body duplication gene, NDC1, leads to aneuploidy and polyploidy. *Proc. Natl. Acad. Sci. USA.* 96:10200–10205. <https://doi.org/10.1073/pnas.96.18.10200>

Cizmecioglu, O., M. Arnold, R. Bahtz, F. Settele, L. Ehret, U. Haselmann-Weiss, C. Antony, and I. Hoffmann. 2010. Cep152 acts as a scaffold for recruitment of Plk4 and CPAP to the centrosome. *J. Cell Biol.* 191:731–739. <https://doi.org/10.1083/jcb.201007107>

Courtois, A., M. Schuh, J. Ellenberg, and T. Hiiragi. 2012. The transition from meiotic to mitotic spindle assembly is gradual during early mammalian development. *J. Cell Biol.* 198:357–370. <https://doi.org/10.1083/jcb.201202135>

Coverley, D., H. Laman, and R.A. Laskey. 2002. Distinct roles for cyclins E and A during DNA replication complex assembly and activation. *Nat. Cell Biol.* 4:523–528. <https://doi.org/10.1038/ncb813>

Debec, A. 1978. Haploid cell cultures of *Drosophila melanogaster*. *Nature.* 274:255–256. <https://doi.org/10.1038/274255a0>

Debec, A. 1984. Evolution of karyotype in haploid cell lines of *Drosophila melanogaster*. *Exp. Cell Res.* 151:236–246. [https://doi.org/10.1016/0014-4827\(84\)90371-9](https://doi.org/10.1016/0014-4827(84)90371-9)

Debec, A., and C. Abbadié. 1989. The acentriolar state of the *Drosophila* cell lines 1182. *Biol. Cell.* 67:307–311. <https://doi.org/10.1111/j.1768-322X.1989.tb00876.x>

Decker, M., S. Jaensch, A. Pozniakovskiy, A. Zinke, K.F. O'Connell, W. Zachariae, E. Myers, and A.A. Hyman. 2011. Limiting amounts of centrosome material set centrosome size in *C. elegans* embryos. *Curr. Biol.* 21:1259–1267. <https://doi.org/10.1016/j.cub.2011.06.002>

Dzhindzhev, N.S., Q.D. Yu, K. Weiskopf, G. Tzolovsky, I. Cunha-Ferreira, M. Riparbelli, A. Rodrigues-Martins, M. Bettencourt-Dias, G. Callaini, and D.M. Glover. 2010. Asterless is a scaffold for the onset of centriole assembly. *Nature.* 467:714–718. <https://doi.org/10.1038/nature09445>

Dzhindzhev, N.S., G. Tzolovsky, Z. Lipinszki, S. Schneider, R. Lattao, J. Fu, J. Debski, M. Dadlez, and D.M. Glover. 2014. Plk4 phosphorylates Ana2 to trigger Sas6 recruitment and procentriole formation. *Curr. Biol.* 24:2526–2532. <https://doi.org/10.1016/j.cub.2014.08.061>

Elling, U., J. Taubenschmid, G. Wirsberger, R. O'Malley, S.P. Demers, Q. Vanhaelen, A.I. Shukalyuk, G. Schmauss, D. Schramek, F. Schnuetgen, et al. 2011. Forward and reverse genetics through derivation of haploid mouse embryonic stem cells. *Cell Stem Cell.* 9:563–574. <https://doi.org/10.1016/j.stem.2011.10.012>

Essletzbichler, P., T. Konopka, F. Santoro, D. Chen, B.V. Gapp, R. Kralovics, T.R. Brummelkamp, S.M. Nijman, and T. Bürckstümmer. 2014. Megabase-scale deletion using CRISPR/Cas9 to generate a fully haploid human cell line. *Genome Res.* 24:2059–2065. <https://doi.org/10.1101/gr.177220.114>

Fong, C.S., M. Kim, T.T. Yang, J.C. Liao, and M.F.B. Tsou. 2014. SAS-6 assembly templated by the lumen of cartwheel-less centrioles precedes centriole duplication. *Dev. Cell.* 30:238–245. <https://doi.org/10.1016/j.devcel.2014.05.008>

Forster, B.P., E. Heberle-Bors, K.J. Kasha, and A. Touraev. 2007. The resurgence of haploids in higher plants. *Trends Plant Sci.* 12:368–375. <https://doi.org/10.1016/j.tplants.2007.06.007>

Freed, J.J. 1962. Continuous cultivation of cells derived from haploid *Rana pipiens* embryos. *Exp. Cell Res.* 26:327–333. [https://doi.org/10.1016/0014-4827\(62\)90185-4](https://doi.org/10.1016/0014-4827(62)90185-4)

Fu, J., Z. Lipinszki, H. Rangone, M. Min, C. Mykura, J. Chao-Chu, S. Schneider, N.S. Dzhindzhev, M. Gottardo, M.G. Riparbelli, et al. 2016. Conserved molecular interactions in centriole-to-centrosome conversion. *Nat. Cell Biol.* 18:87–99. <https://doi.org/10.1038/ncb3274>

Ganem, N.J., S.A. Godinho, and D. Pellman. 2009. A mechanism linking extra centrosomes to chromosomal instability. *Nature.* 460:278–282. <https://doi.org/10.1038/nature08136>

Godinho, S.A., and D. Pellman. 2014. Causes and consequences of centrosome abnormalities in cancer. *Philos. Trans. R. Soc. Lond. B Biol. Sci.* 369:20130467. <https://doi.org/10.1098/rstb.2013.0467>

Godinho, S.A., R. Picone, M. Burute, R. Dagher, Y. Su, C.T. Leung, K. Polyak, J.S. Brugge, M. Théry, and D. Pellman. 2014. Oncogene-like induction of cellular invasion from centrosome amplification. *Nature.* 510:167–171. <https://doi.org/10.1038/nature13277>

Gönczy, P. 2015. Centrosomes and cancer: revisiting a long-standing relationship. *Nat. Rev. Cancer.* 15:639–652. <https://doi.org/10.1038/nrc3995>

Gueth-Hallonet, C., C. Antony, J. Aghion, A. Santa-Maria, I. Lajoie-Mazenc, M. Wright, and B. Maro. 1993. gamma-Tubulin is present in acentriolar MTOCs during early mouse development. *J. Cell Sci.* 105:157–166.

- Habedanck, R., Y.D. Stierhof, C.J. Wilkinson, and E.A. Nigg. 2005. The Polo kinase Plk4 functions in centriole duplication. *Nat. Cell Biol.* 7:1140–1146. <https://doi.org/10.1038/ncb1320>
- Hasegawa, K., S.J. Ryu, and P. Kaláb. 2013. Chromosomal gain promotes formation of a steep RanGTP gradient that drives mitosis in aneuploid cells. *J. Cell Biol.* 200:151–161. <https://doi.org/10.1083/jcb.201206142>
- Hatch, E.M., A. Kulukian, A.J. Holland, D.W. Cleveland, and T. Stearns. 2010. Cep152 interacts with Plk4 and is required for centriole duplication. *J. Cell Biol.* 191:721–729. <https://doi.org/10.1083/jcb.201006049>
- Kaufman, M.H. 1978. Chromosome analysis of early postimplantation presumptive haploid parthenogenetic mouse embryos. *J. Embryol. Exp. Morphol.* 45:85–91.
- Khodjakov, A., and C.L. Rieder. 2001. Centrosomes enhance the fidelity of cytokinesis in vertebrates and are required for cell cycle progression. *J. Cell Biol.* 153:237–242. <https://doi.org/10.1083/jcb.153.1.237>
- Khodjakov, A., R.W. Cole, B.R. Oakley, and C.L. Rieder. 2000. Centrosome-independent mitotic spindle formation in vertebrates. *Curr. Biol.* 10:59–67. [https://doi.org/10.1016/S0960-9822\(99\)00276-6](https://doi.org/10.1016/S0960-9822(99)00276-6)
- Kim, H.-T., M.-S. Lee, J.-H. Choi, J.-Y. Jung, D.-G. Ahn, S.-Y. Yeo, D.-K. Choi, and C.-H. Kim. 2011. The microcephaly gene *aspm* is involved in brain development in zebrafish. *Biochem. Biophys. Res. Commun.* 409:640–644. <https://doi.org/10.1016/j.bbrc.2011.05.056>
- Kim, J., K. Lee, and K. Rhee. 2015. PLK1 regulation of PCNT cleavage ensures fidelity of centriole separation during mitotic exit. *Nat. Commun.* 6:10076. <https://doi.org/10.1038/ncomms10076>
- Kim, T.S., J.E. Park, A. Shukla, S. Choi, R.N. Murugan, J.H. Lee, M. Ahn, K. Rhee, J.K. Bang, B.Y. Kim, et al. 2013. Hierarchical recruitment of Plk4 and regulation of centriole biogenesis by two centrosomal scaffolds, Cep192 and Cep152. *Proc. Natl. Acad. Sci. USA.* 110:E4849–E4857. <https://doi.org/10.1073/pnas.1319656110>
- Kishigami, S., and T. Wakayama. 2007. Efficient strontium-induced activation of mouse oocytes in standard culture media by chelating calcium. *J. Reprod. Dev.* 53:1207–1215. <https://doi.org/10.1262/jrd.19067>
- Kleylein-Sohn, J., J. Westendorf, M. Le Clech, R. Habedanck, Y.D. Stierhof, and E.A. Nigg. 2007. Plk4-induced centriole biogenesis in human cells. *Dev. Cell.* 13:190–202. <https://doi.org/10.1016/j.devcel.2007.07.002>
- Ko, M.A., C.O. Rosario, J.W. Hudson, S. Kulkarni, A. Pollett, J.W. Dennis, and C.J. Swallow. 2005. Plk4 haploinsufficiency causes mitotic infidelity and carcinogenesis. *Nat. Genet.* 37:883–888. <https://doi.org/10.1038/ng1605>
- Kotecki, M., P.S. Reddy, and B.H. Cochran. 1999. Isolation and characterization of a near-haploid human cell line. *Exp. Cell Res.* 252:273–280. <https://doi.org/10.1006/excr.1999.4656>
- Kuriyama, R., and G.G. Borisy. 1981. Centriole cycle in Chinese hamster ovary cells as determined by whole-mount electron microscopy. *J. Cell Biol.* 91:814–821. <https://doi.org/10.1083/jcb.91.3.814>
- Latham, K.E., H. Akutsu, B. Patel, and R. Yanagimachi. 2002. Comparison of gene expression during preimplantation development between diploid and haploid mouse embryos. *Biol. Reprod.* 67:386–392. <https://doi.org/10.1095/biolreprod67.2.386>
- Lee, K., and K. Rhee. 2012. Separate-dependent cleavage of pericentriolar B is necessary and sufficient for centriole disengagement during mitosis. *Cell Cycle.* 11:2476–2485. <https://doi.org/10.4161/cc.20878>
- Leeb, M., and A. Wutz. 2011. Derivation of haploid embryonic stem cells from mouse embryos. *Nature.* 479:131–134. <https://doi.org/10.1038/nature10448>
- Leidel, S., M. Delattre, L. Cerutti, K. Baumer, and P. Gönczy. 2005. SAS-6 defines a protein family required for centrosome duplication in *C. elegans* and in human cells. *Nat. Cell Biol.* 7:115–125. <https://doi.org/10.1038/ncb1220>
- Li, W., X. Li, T. Li, M.G. Jiang, H. Wan, G.Z. Luo, C. Feng, X. Cui, F. Teng, Y. Yuan, et al. 2014. Genetic modification and screening in rat using haploid embryonic stem cells. *Cell Stem Cell.* 14:404–414. <https://doi.org/10.1016/j.stem.2013.11.016>
- Liu, L., J.R. Trimarchi, and D.L. Keefe. 2002. Haploidy but not parthenogenetic activation leads to increased incidence of apoptosis in mouse embryos. *Biol. Reprod.* 66:204–210. <https://doi.org/10.1095/biolreprod66.1.204>
- Loncerek, J., and M. Bettencourt-Dias. 2018. Building the right centriole for each cell type. *J. Cell Biol.* 217:823–835.
- Luo, C., and B. Li. 2003. Diploid-dependent regulation of gene expression: a genetic cause of abnormal development in fish haploid embryos. *Heredity (Edinb)*. 90:405–409. <https://doi.org/10.1038/sj.hdy.6800263>
- Mable, B.K., and S.P. Otto. 1998. The evolution of life cycles with haploid and diploid phases. *BioEssays.* 20:453–462. [https://doi.org/10.1002/\(SICI\)1521-1878\(199806\)20:6%3C453::AID-BIES3%3E3.0.CO;2-N](https://doi.org/10.1002/(SICI)1521-1878(199806)20:6%3C453::AID-BIES3%3E3.0.CO;2-N)
- Matsumoto, Y., K. Hayashi, and E. Nishida. 1999. Cyclin-dependent kinase 2 (Cdk2) is required for centrosome duplication in mammalian cells. *Curr. Biol.* 9:429–432. [https://doi.org/10.1016/S0960-9822\(99\)80191-2](https://doi.org/10.1016/S0960-9822(99)80191-2)
- Matsuo, K., K. Ohsumi, M. Iwabuchi, T. Kawamata, Y. Ono, and M. Takahashi. 2012. Kendrin is a novel substrate for separase involved in the licensing of centriole duplication. *Curr. Biol.* 22:915–921. <https://doi.org/10.1016/j.cub.2012.03.048>
- McNally, F.J. 2013. Mechanisms of spindle positioning. *J. Cell Biol.* 200:131–140. <https://doi.org/10.1083/jcb.201210007>
- Meraldi, P., J. Lukas, A.M. Fry, J. Bartek, and E.A. Nigg. 1999. Centrosome duplication in mammalian somatic cells requires E2F and Cdk2-cyclin A. *Nat. Cell Biol.* 1:88–93. <https://doi.org/10.1038/10054>
- Moyer, T.C., K.M. Clutario, B.G. Lambrus, V. Daggubati, and A.J. Holland. 2015. Binding of STIL to Plk4 activates kinase activity to promote centriole assembly. *J. Cell Biol.* 209:863–878. <https://doi.org/10.1083/jcb.201502088>
- Nakazawa, Y., M. Hiraki, R. Kamiya, and M. Hirono. 2007. SAS-6 is a cartwheel protein that establishes the 9-fold symmetry of the centriole. *Curr. Biol.* 17:2169–2174. <https://doi.org/10.1016/j.cub.2007.11.046>
- Nasmyth, K. 2002. Segregating sister genomes: the molecular biology of chromosome separation. *Science.* 297:559–565. <https://doi.org/10.1126/science.1074757>
- Novorol, C., J. Burkhardt, K.J. Wood, A. Iqbal, C. Roque, N. Coutts, A.D. Almeida, J. He, C.J. Wilkinson, and W.A. Harris. 2013. Microcephaly models in the developing zebrafish retinal neuroepithelium point to an underlying defect in metaphase progression. *Open Biol.* 3:130065. <https://doi.org/10.1098/rsob.130065>
- Oakley, B.R., V. Paolillo, and Y. Zheng. 2015.  $\gamma$ -Tubulin complexes in microtubule nucleation and beyond. *Mol. Biol. Cell.* 26:2957–2962. <https://doi.org/10.1091/mbc.E14-11-1514>
- Ohta, M., T. Ashikawa, Y. Nozaki, H. Kozuka-Hata, H. Goto, M. Inagaki, M. Oyama, and D. Kitagawa. 2014. Direct interaction of Plk4 with STIL ensures formation of a single procentriole per parental centriole. *Nat. Commun.* 5:5267. <https://doi.org/10.1038/ncomms6267>
- Pagan, J.K., A. Marzio, M.J. Jones, A. Saraf, P.V. Jallepalli, L. Florens, M.P. Washburn, and M. Pagano. 2015. Degradation of Cep68 and PCNT cleavage mediate Cep215 removal from the PCM to allow centriole separation, disengagement and licensing. *Nat. Cell Biol.* 17:31–43. <https://doi.org/10.1038/ncb3076>
- Park, S.-Y., J.-E. Park, T.-S. Kim, J.H. Kim, M.-J. Kwak, B. Ku, L. Tian, R.N. Murugan, M. Ahn, S. Komiya, et al. 2014. Molecular basis for unidirectional scaffold switching of human Plk4 in centriole biogenesis. *Nat. Struct. Mol. Biol.* 21:696–703. <https://doi.org/10.1038/nsmb.2846>
- Patton, E.E., and L.I. Zon. 2001. The art and design of genetic screens: zebrafish. *Nat. Rev. Genet.* 2:956–966. <https://doi.org/10.1038/35103567>
- Peel, N., N.R. Stevens, R. Basto, and J.W. Raff. 2007. Overexpressing centriole-replication proteins in vivo induces centriole overduplication and de novo formation. *Curr. Biol.* 17:834–843. <https://doi.org/10.1016/j.cub.2007.04.036>
- Petretti, C., M. Savoian, E. Montembault, D.M. Glover, C. Prigent, and R. Giet. 2006. The PITSLRE/CDK1p58 protein kinase promotes centrosome maturation and bipolar spindle formation. *EMBO Rep.* 7:418–424.
- Piel, M., P. Meyer, A. Khodjakov, C.L. Rieder, and M. Bornens. 2000. The respective contributions of the mother and daughter centrosomes to centrosome activity and behavior in vertebrate cells. *J. Cell Biol.* 149:317–330. <https://doi.org/10.1083/jcb.149.2.317>
- Potapova, T.A., C.W. Seidel, A.C. Box, G. Rancati, and R. Li. 2016. Transcriptome analysis of tetraploid cells identifies cyclin D2 as a facilitator of adaptation to genome doubling in the presence of p53. *Mol. Biol. Cell.* 27:3065–3084. <https://doi.org/10.1091/mbc.E16-05-0268>
- Rhys, A.D., P. Monteiro, C. Smith, M. Vaghela, T. Arnanadis, T. Kato, B. Leitinger, E. Sahai, A. McAinsh, G. Charras, and S.A. Godinho. 2018. Loss of E-cadherin provides tolerance to centrosome amplification in epithelial cancer cells. *J. Cell Biol.* 217:195–209. <https://doi.org/10.1083/jcb.201704102>
- Sagi, I., G. Chia, T. Golan-Lev, M. Peretz, U. Weissbein, L. Sui, M.V. Sauer, O. Yanuka, D. Egli, and N. Benvenisty. 2016. Derivation and differentiation of haploid human embryonic stem cells. *Nature.* 532:107–111. <https://doi.org/10.1038/nature17408>
- Seo, M.Y., W. Jang, and K. Rhee. 2015. Integrity of the Pericentriolar Material Is Essential for Maintaining Centriole Association during M Phase. *PLoS One.* 10:e0138905. <https://doi.org/10.1371/journal.pone.0138905>
- Sir, J.H., M. Pütz, O. Daly, C.G. Morrison, M. Dunning, J.V. Kilmartin, and F. Gergely. 2013. Loss of centrioles causes chromosomal instability in

- vertebrate somatic cells. *J. Cell Biol.* 203:747–756. <https://doi.org/10.1083/jcb.201309038>
- Sonnen, K.F., A.M. Gabryjarczyk, E. Anselm, Y.D. Stierhof, and E.A. Nigg. 2013. Human Cep192 and Cep152 cooperate in Plk4 recruitment and centriole duplication. *J. Cell Sci.* 126:3223–3233. <https://doi.org/10.1242/jcs.129502>
- Sumara, I., E. Vorlaufer, P.T. Stukenberg, O. Kelm, N. Redemann, E.A. Nigg, and J.M. Peters. 2002. The dissociation of cohesin from chromosomes in prophase is regulated by Polo-like kinase. *Mol. Cell.* 9:515–525. [https://doi.org/10.1016/S1097-2765\(02\)00473-2](https://doi.org/10.1016/S1097-2765(02)00473-2)
- Szöllösi, A., H. Ris, D. Szöllösi, and A. Debec. 1986. A centriole-free *Drosophila* cell line. A high voltage EM study. *Eur. J. Cell Biol.* 40:100–104.
- Tsou, M.F., and T. Stearns. 2006. Mechanism limiting centrosome duplication to once per cell cycle. *Nature.* 442:947–951. <https://doi.org/10.1038/nature04985>
- Tsou, M.F., W.J. Wang, K.A. George, K. Uryu, T. Stearns, and P.V. Jallepalli. 2009. Polo kinase and separase regulate the mitotic licensing of centriole duplication in human cells. *Dev. Cell.* 17:344–354. <https://doi.org/10.1016/j.devcel.2009.07.015>
- Uehara, R., and G. Goshima. 2010. Functional central spindle assembly requires de novo microtubule generation in the interchromosomal region during anaphase. *J. Cell Biol.* 191:259–267. <https://doi.org/10.1083/jcb.201004150>
- Uehara, R., R.S. Nozawa, A. Tomioka, S. Petry, R.D. Vale, C. Obuse, and G. Goshima. 2009. The augmin complex plays a critical role in spindle microtubule generation for mitotic progression and cytokinesis in human cells. *Proc. Natl. Acad. Sci. USA.* 106:6998–7003. <https://doi.org/10.1073/pnas.0901587106>
- Uehara, R., T. Kamasaki, S. Hiruma, I. Poser, K. Yoda, J. Yajima, D.W. Gerlich, and G. Goshima. 2016. Augmin shapes the anaphase spindle for efficient cytokinetic furrow ingression and abscission. *Mol. Biol. Cell.* 27:812–827. <https://doi.org/10.1091/mbc.E15-02-0101>
- Uetake, Y., and G. Sluder. 2010. Prolonged prometaphase blocks daughter cell proliferation despite normal completion of mitosis. *Curr. Biol.* 20:1666–1671. <https://doi.org/10.1016/j.cub.2010.08.018>
- Wong, Y.L., J.V. Anzola, R.L. Davis, M. Yoon, A. Motamedi, A. Kroll, C.P. Seo, J.E. Hsia, S.K. Kim, J.W. Mitchell, et al. 2015. Cell biology. Reversible centriole depletion with an inhibitor of Polo-like kinase 4. *Science.* 348:1155–1160. <https://doi.org/10.1126/science.aaa5111>
- Wutz, A. 2014. Haploid animal cells. *Development.* 141:1423–1426. <https://doi.org/10.1242/dev.102202>
- Yang, H., Z. Liu, Y. Ma, C. Zhong, Q. Yin, C. Zhou, L. Shi, Y. Cai, H. Zhao, H. Wang, et al. 2013. Generation of haploid embryonic stem cells from *Macaca fascicularis* monkey parthenotes. *Cell Res.* 23:1187–1200. <https://doi.org/10.1038/cr.2013.93>
- Yokoyama, H., O.J. Gruss, S. Rybina, M. Caudron, M. Schelder, M. Wilm, I.W. Mattaj, and E. Karsenti. 2008. Cdk1 is a RanGTP-dependent microtubule stabilization factor that regulates spindle assembly rate. *J. Cell Biol.* 180:867–875. <https://doi.org/10.1083/jcb.200706189>

Supplemental material

Yaguchi et al., <https://doi.org/10.1083/jcb.201701151>

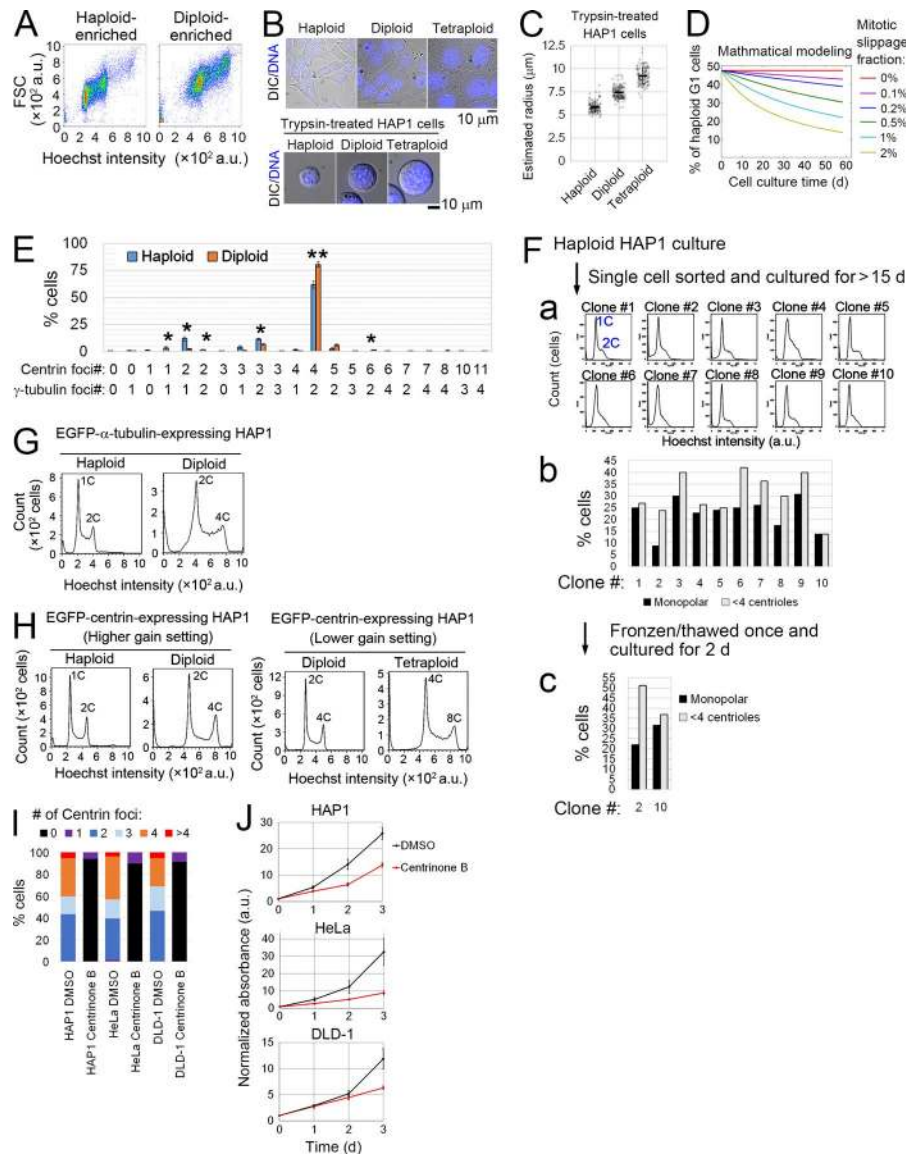
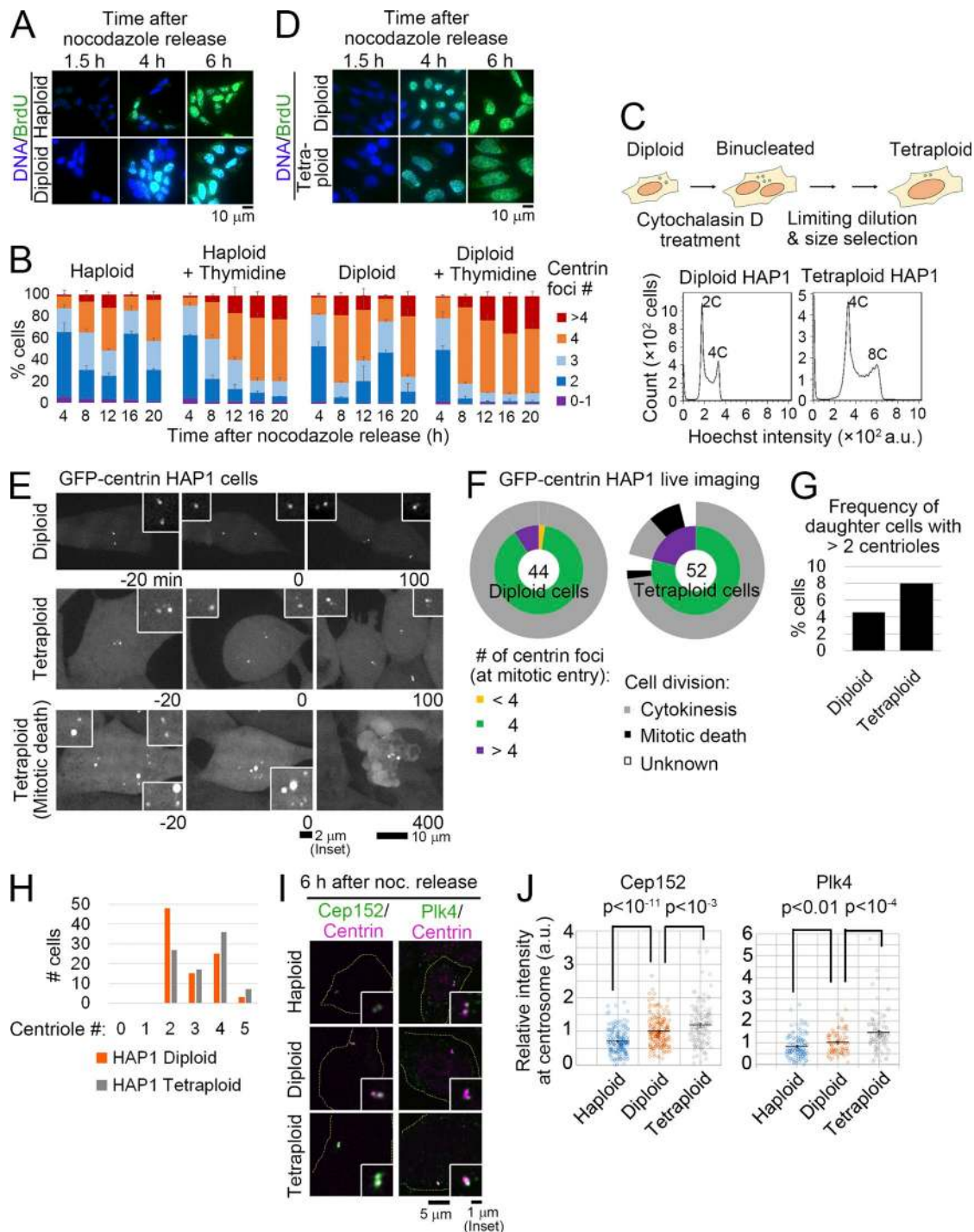


Figure S1. **Analysis of isogenic HAP1 cell lines with different ploidies.** (A) Flow cytometric analysis of FSC and DNA content in Hoechst-stained haploid or diploid HAP1 cells. (B) Microscopy of adhesive (top) or trypsin-treated (bottom) haploid, diploid, or tetraploid HAP1 cells. DNA was stained using Hoechst. (C) Radii of trypsin-treated haploid, diploid, or tetraploid HAP1 cells, estimated using measured values of cell area. Values represent means  $\pm$  SD of at least 125 cells from two independent experiments per condition. There were significant differences between all pairs of samples ( $P < 10^{-50}$ , *t* test). (D) Time plots of simulated haploid G1 fractions during long-term culture of haploid enriched cell populations with different frequencies of mitotic slippage. Note that neither haploid-specific cell cycle delay nor mitotic death was taken into account in these simulations. (E) Distribution of centriole and centrosome number in mitotic haploid and diploid HAP1 cells shown in Fig. 2 D. Values represent means  $\pm$  SE of three independent experiments. Statistically significant differences between haploid and diploid cells are indicated by asterisks (\*,  $P < 0.05$ ; \*\*,  $P < 0.01$ , *t* test). At least 302 cells were analyzed per condition. (F) Haploid cells were single-cell sorted, and 10 individual clonal populations were expanded for more than 15 d. Each clone was subjected to flow cytometric analysis of DNA content (a), or immunostaining of  $\alpha$ -tubulin and centrin to quantify the frequency of spindle monopolarization and centriole loss (b). The immunostaining analysis was repeated in clones 2 and 10, which showed relatively low frequency of spindle/centrosome defects (c). At least 19 cells were analyzed for each clone. (G and H) Flow cytometric analysis of DNA content in Hoechst-stained haploid or diploid HAP1 cells stably expressing EGFP- $\alpha$ -tubulin (G) or GFP-centrin (H). GFP-centrin lines were analyzed using two different gain settings. Representative data from at least two independent experiments are shown in A, G, and H. (I) Quantification of centrin-positive dots in HAP1, HeLa, and DLD-1 cells that were treated with or without 0.5–1  $\mu$ M centrinone B for >14 d. At least 46 cells from two independent experiments were analyzed. (J) Effect of chronic centrosome loss, which was induced by the long-term centrinone B treatment, on cell growth in different cell lines. Cells were seeded in 96-well plates at 2,500, 750, or 1,250 cells/well (for HAP1, HeLa, or DLD-1 cells, respectively) on day 0, and their growth was quantified by the CCK-8 assay. For each condition, absorbance at 450 nm measured on days 0–3 was normalized to that on day 0. Values represent mean  $\pm$  SE of six samples from two independent experiments.



**Figure S2. Ploidy-dependent changes in centrosome duplication efficiency.** (A and D) Immunostaining of incorporated BrdU in synchronized HAP1 cells with different ploidy. DNA was stained with DAPI. (B) Percentages of haploid or diploid cells with indicated numbers of centrin foci at each time point after nocodazole release. Cells were incubated with or without 4 mM thymidine. Values represent mean  $\pm$  SE of three independent experiments. At least 161 cells were analyzed for each data point. (C) A schematic of the procedure for the establishment of tetraploid HAP1 cells (top), and flow cytometric analysis of DNA content in Hoechst-stained diploid or tetraploid HAP1 cells (bottom). Representative data from two independent experiments are shown. (E) Live images of diploid or tetraploid GFP-centrin cells. Images were taken at 20-min intervals. Insets: 2 $\times$  enlarged images of centrioles. (F) Classification of mitotic defects (outer circle) sorted by centriole content (inner circle) in E. At least 44 GFP-centrin cells from two independent experiments were analyzed. Mitotic cells that moved out of the field of view or did not exit mitosis by the end of imaging were categorized as unknown. (G) Frequency of daughter cells with more than two centrioles in E. At least 88 daughter cells from two independent experiments were analyzed. (H) Frequency of centrin-positive foci number in immunostaining of asynchronous diploid or tetraploid HAP1 cells. At least 87 cells from two independent experiments were analyzed. (I) Immunostaining of centrosome proteins in synchronized HAP1 cells with different ploidy. Broken lines indicate boundaries of cells or nuclei. Insets: 2.5 $\times$  enlarged images of the centrioles. (J) Normalized intensities of centrosome proteins at the centrosomes in I. Values represent mean  $\pm$  SE of at least 65 centrioles from two independent experiments for each condition ( $p$ -values calculated using  $t$  tests are shown).



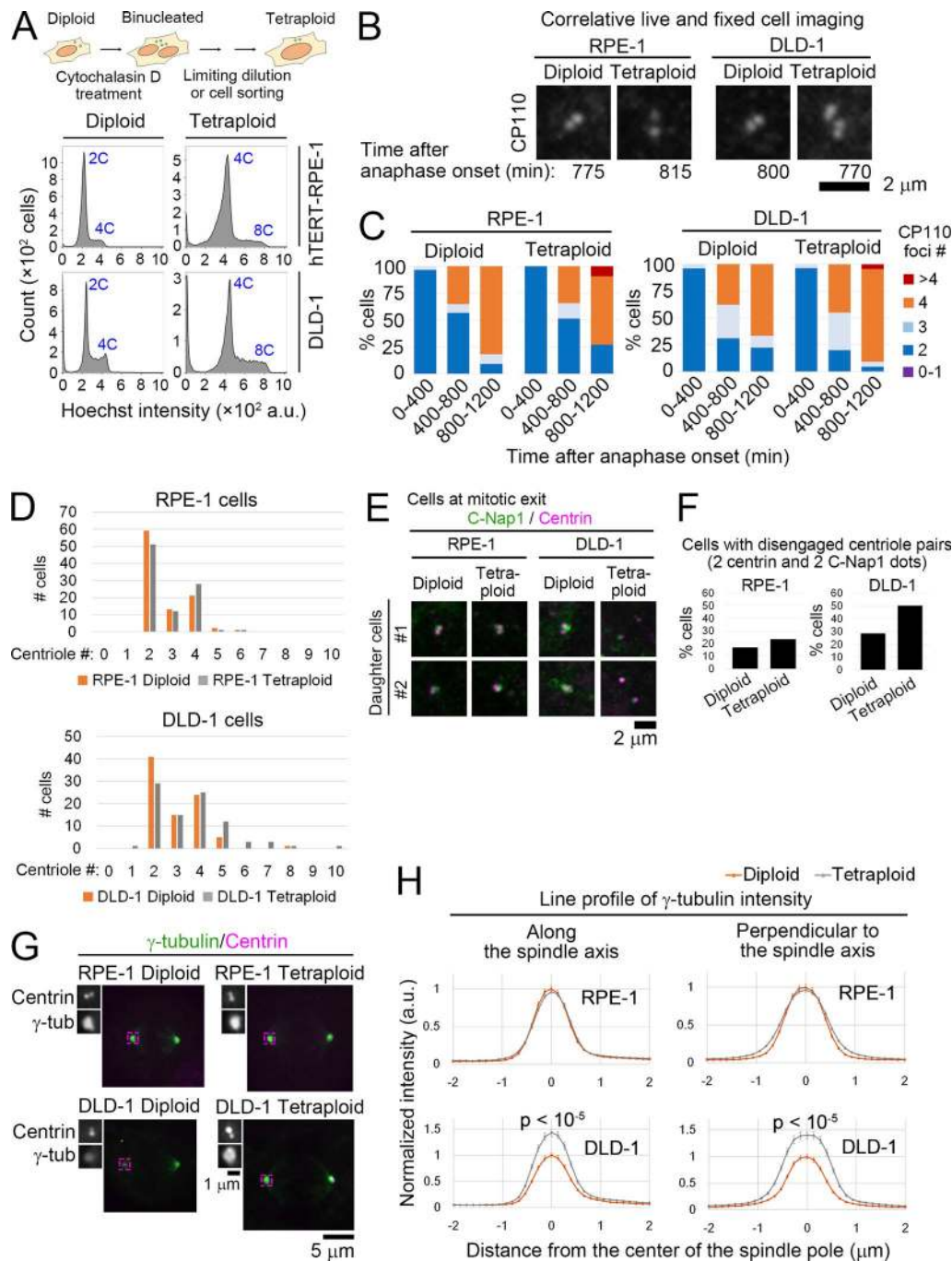


Figure S3. **Centrosome cycle in isogenic diploid and tetraploid RPE-1 or DLD-1 cells.** (A) A schematic of the procedure for the establishment of tetraploid RPE-1 or DLD-1 cells (top), and flow cytometric analysis of DNA content in Hoechst-stained diploid or tetraploid cells (bottom). Representative data from two independent experiments are shown. (B) Immunostaining of CP110 in diploid and tetraploid RPE-1 or DLD-1 cells in the correlative live- and fixed-cell imaging. Cells were fixed and immunostained for CP110 after 24-h DIC live imaging. Enlarged images of the centrioles are shown. (C) Percentages of cells with indicated numbers of CP110 foci at each time window after anaphase onset in B. At least 70 cells from at least two independent experiments were analyzed for each condition (at least 11 cells for each data point). (D) Frequency of centrin-positive foci number in immunostaining of asynchronous diploid and tetraploid RPE-1 or DLD-1 cells. At least 86 cells from two independent experiments were analyzed. Although the difference in mean centriole number between diploid and tetraploid DLD-1 cells may partially arise from potential difference in their cell cycle stage distribution, the prominent increase in the frequency of supernumerary centriole in tetraploid DLD-1 indicates tetraploidy-linked up-regulation of centriole duplication in this cell line. (E) Immunostaining of centrin and C-Nap1 in diploid and tetraploid RPE-1 or DLD-1 cells at mitotic exit. Enlarged images of the centrioles are shown. (F) Frequencies of cells with disengaged centriole pairs (with two centrin and two C-Nap1 dots) in E. At least 81 cells from two independent experiments were analyzed. (G) Immunostaining of  $\gamma$ -tubulin and centrin in preanaphase RPE-1 or DLD-1 cells with different ploidies. Insets show 2 $\times$  enlarged images of centrin or  $\gamma$ -tubulin at the spindle poles indicated by magenta boxes. (H) Line profiles of  $\gamma$ -tubulin at the spindle poles in G. Spindle poles with two centrioles were analyzed. Values represent mean  $\pm$  SE of at least 50 spindle poles from three independent experiments. In DLD-1 cells,  $\gamma$ -tubulin intensity at the center of the spindle pole was significantly higher in tetraploid state than in diploid ( $p$ -values calculated using  $t$  tests are shown).

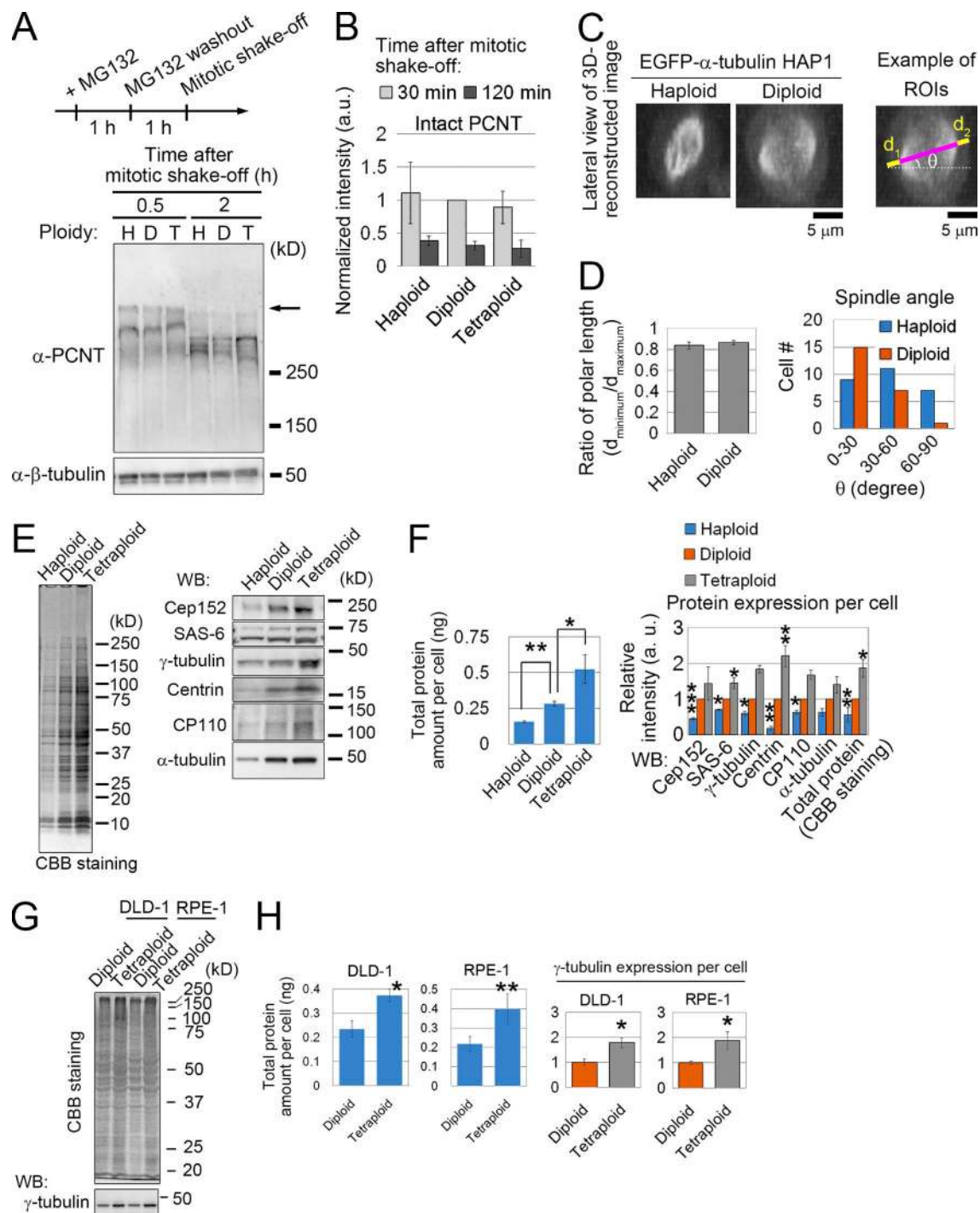


Figure S4. **Comparison of PCNT degradation, spindle positioning, or protein expression among different ploidy states.** (A) IB of PCNT after MG132 release and mitotic shake-off in HAP1 cells with different ploidy.  $\beta$ -tubulin was detected as a loading control. Arrow indicates intact PCNT. (B) Quantification of the IB signal of intact PCNT normalized to that of  $\beta$ -tubulin in A. Values represent mean  $\pm$  SE of three independent experiments. There was no significant difference in the normalized intensity among different ploidy states (*t* test). (C) Left: Lateral view of 3D reconstructed image of haploid or diploid EGFP- $\alpha$ -tubulin HAP1 cells. Right: An example of ROIs for the quantification in D. (D) Left: Comparison of spindle positioning symmetry between haploid and diploid cells. The ratio of polar length (distance between polar cortex and a proximal spindle pole) was measured as depicted in C. Values represent mean  $\pm$  SE of at least 23 cells from two independent experiments. There was no statistically significant difference in the symmetry of spindle position between haploid and diploid cells (*t* test). Right: Distribution of spindle angle measured as depicted in C. Spindle angle was significantly larger in haploid cells than in diploid ( $P < 0.01$ , *t* test). Twenty-seven haploid and 23 diploid cells from two independent experiments were analyzed. (E and G) Coomassie brilliant blue (CBB) staining of total protein (left in E, and top in G) and IB of centrosomal proteins (right in E, and bottom in G) in equivalent numbers of haploid, diploid, and tetraploid HAP1 (E), DLD-1, or RPE-1 cells (G). (F and H) Quantification of total proteins in E (left in F) or G (top in H), or normalized IB signal intensities in E (right in F) or G (bottom in H). Values represent mean  $\pm$  SE of three independent experiments (asterisks indicate significant differences from diploid cells; \*,  $P < 0.05$ ; \*\*,  $P < 0.01$ ; \*\*\*,  $P < 0.001$ , *t* test).

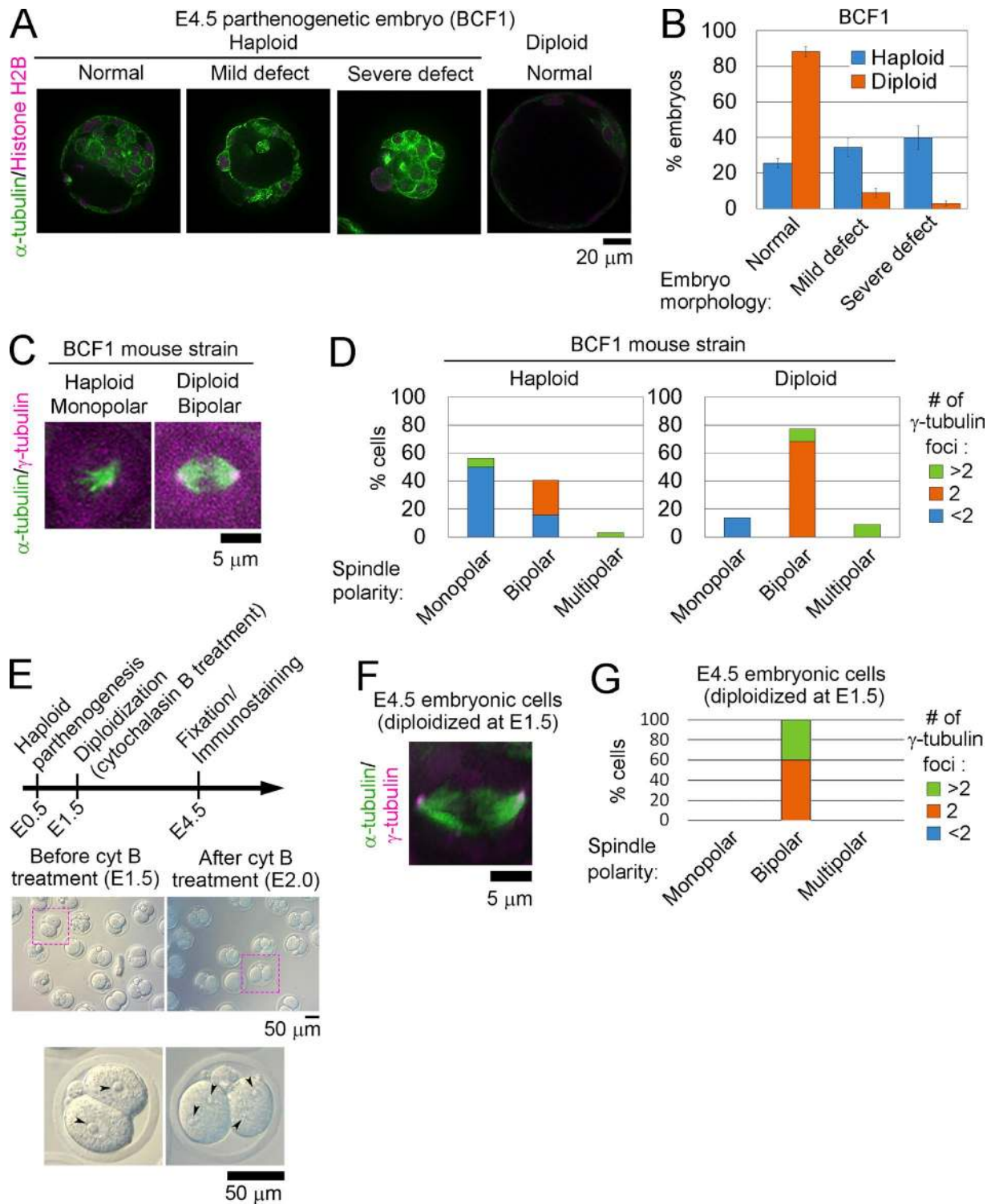
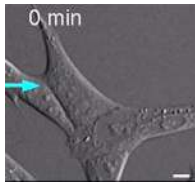
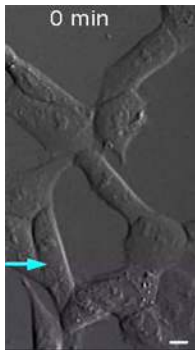


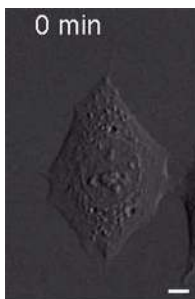
Figure S5. **Centrosome loss and monopolar spindle formation in mouse haploid embryos.** (A, C, and F) Immunostaining of  $\alpha$ -tubulin and histone H2B (A), or  $\gamma$ -tubulin (C, F) in haploid and diploid mouse parthenogenetic embryos (stage E4.5) from BCF1 strain (A and C), or B6D2F1 parthenogenetic embryos diploidized at E1.5 and fixed at E4.5 (F). Enlarged mitotic cells in the embryos are shown in C and F. (B) Frequencies of morphological abnormalities in A. Values represent mean  $\pm$  SE of three independent experiments. At least 71 embryos were analyzed per condition. (D and G) Frequency of spindle polarities and centrosome numbers in C (D) or F (G). At least 22 cells from 18 embryos from 3 independent experiments (D), or 10 cells from 10 embryos from 3 independent experiments (G) were analyzed per condition. (E) Top: Schematic of the procedure for diploidization of haploid embryos at E1.5. Note that de novo centriole biogenesis reportedly occurs at around E3.5, which is after the completion of diploidization. Middle: Haploid parthenogenetic embryos before and after cytochalasin B treatment at E1.5. Embryos indicated by magenta boxes were enlarged in the bottom panels. Arrowheads indicate nuclei.



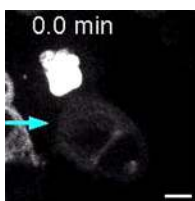
Video 1. **Live imaging of a haploid HAP1 cell that completed cell division (blue arrow).** DIC microscopy of asynchronous culture of haploid HAP1 cells taken at 5-min intervals (shown at 7 frames/s). Pink arrows indicate daughter cells. Bar, 5  $\mu$ m.



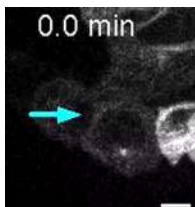
Video 2. **Live imaging of a haploid HAP1 cell that underwent mitotic slippage (blue arrow).** DIC microscopy of asynchronous culture of haploid HAP1 cells taken at 5-min intervals (shown at 7 frames/s). Bar, 5  $\mu$ m.



Video 3. **Live imaging of a diploid HAP1 cell that completed cell division.** DIC microscopy of asynchronous culture of diploid HAP1 cells taken at 5-min intervals (shown at 7 frames/s). Bar, 5  $\mu$ m.



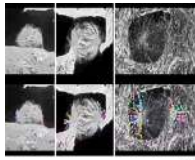
Video 4. **Live imaging of a haploid HAP1 EGFP- $\alpha$ -tubulin cell with the bipolar spindle (blue arrow).** Confocal microscopy of asynchronous culture of haploid GFP- $\alpha$ -tubulin HAP1 cells taken at 12.5-min intervals (shown at 7 frames/s). Pink arrows indicate daughter cells. Bar, 5  $\mu$ m.



Video 5. **Live imaging of a haploid HAP1 EGFP- $\alpha$ -tubulin cells, in which the monopolar spindle later converted to bipolar (blue arrow).** Confocal microscopy of asynchronous culture of haploid GFP- $\alpha$ -tubulin HAP1 cells taken at 12.5-min intervals (shown at 7 frames/s). Pink arrows indicate daughter cells. Bar, 5  $\mu$ m.



Video 6. **Live imaging of a haploid HAP1 EGFP- $\alpha$ -tubulin cell that underwent mitotic slippage (blue arrow).** Confocal microscopy of asynchronous culture of haploid GFP- $\alpha$ -tubulin HAP1 cells taken at 12.5-min intervals (shown at 7 frames/s). Bar, 5  $\mu$ m.



Video 7. **Examples of astral MT tracing for the quantification in Fig. 9 B.** 3D reconstruction of confocal microscopy of HAP1 cells immunostained for  $\alpha$ -tubulin (shown at 7 frames/s). Bar, 5  $\mu$ m.

Table S1. **Parameters and constants used in the simulations**

Constants (unit)	Meaning	Cell cycle delay, mitotic slippage, and mitotic death (Fig. 1 G)	Cell cycle delay and mitotic death (Fig. 1 G)	Mitotic slippage (Fig. 1 G)	Fig. S1 D
$N_{haploid}(0) \times (\times 10^3 \times \text{cells})$	Initial number of haploid cells	5	5	5	5
$N_{diploid}(0) \times (\times 10^3 \times \text{cells})$	Initial number of diploid cells	0	0	0	0
$q_{slippage}$ (h)	Incidence rate of mitotic slippage per mitotic event	0.59	0	0.59	0–2
$q_{death}$ (h)	Incidence rate of mitotic death per mitotic event	1.6	1.6	0	0
$\tau_{haploid}$ (h)	Cell cycle length of haploid	13.4	13.4	11.9	11.9
$\tau_{diploid}$ (h)	Cell cycle length of diploid	11.9	11.9	11.9	11.9
$F_{haploid,G1}$ (%)	G1 cell fraction within haploid population	47.7	47.7	47.7	47.7

Provided online are source code files used in the simulation for modeling dynamics of haploid cell population (DataS1.txt) and for drawing plots (DataS2.txt).